Spheroidization of Iron Powders by Radiative Heat Transfer

by

Rodrigo Javier Quintero de la Garza

S.B. Mechanical and Electrical Engineering
Instituto Tecnológico y de Estudios Superiores de Monterrey, 1995

Submitted to the Department of Materials Science and Engineering
and the Department of Mechanical Engineering in Partial Fulfillment
of the Requirements for the Degrees of

MASTER OF SCIENCE IN MATERIALS SCIENCE AND ENGINEERING
and
MASTER OF SCIENCE IN MECHANICAL ENGINEERING

at the
MASSACHUSETTS INSTITUTE OF TECHNOLOGY
June, 1999

Signature of Author .....
Department of Materials Science and Engineering
May 7, 1999

Certified by .....
Thomas W. Eagar
POSCO Professor of Materials Engineering
Thesis Supervisor

Certified by .....
Jung-Hoon Chun
Associate Professor of Mechanical Engineering
Thesis Reader

Accepted by .....
Linn W. Hobbs
John Elliot Professor of Materials
Chairman, Departmental Committee on Graduate Students

Accepted by .....
Ain A. Sonin
Professor of Mechanical Engineering
Chairman, Departmental Committee on Graduate Students

Spheroidization of Iron Powders by Radiative Heat Transfer

by

Rodrigo Javier Quintero de la Garza

Submitted to the Department of Materials Science and Engineering and the Department of Mechanical Engineering on May 7, 1999 in Partial Fulfillment of the Requirements for the Degrees of Master of Science in Materials Science and Engineering and Master of Science in Mechanical Engineering.

ABSTRACT

An experimental study was performed to produce spherical iron powders from irregularly shaped water atomized powders. This process consists of re-melting the water atomized powders in a drop tube at temperatures above the particles' melting point. The proposed process consists of a drop tube heated by electric resistors in which small irregularly shaped iron particles rapidly melt by thermal radiation and form spherical particles by means of surface tension. Since the process is carried out in a vacuum, convective heat transfer is negligible compared to the radiative heat transfer.

Although this technique has been used in the past to produce single particles, its use to mass-produce spherical iron powder has not been employed. The purpose of this work is to extend this process to mass-production of spherical iron powder from atomized powders and to develop a better understanding of this technique and its application to processing iron or other iron alloy powders.

Laboratory tests proved this process successful to spheroidize irregularly shaped particles at low feed rates, however, this process can be easily adapted to produce larger quantities of material without significant changes in equipment configuration.

Thesis Supervisor: Thomas W. Eagar
Title: POSCO Professor of Materials Engineering

Thesis Reader: Jung-Hoon Chun
Title: Associate Professor of Mechanical Engineering

Acknowledgments

I would like to thank every person who helped me complete my thesis and studies at MIT. First and foremost, I want to thank Professor Thomas Eagar for giving me the opportunity to work in this project. I will be always be grateful for his support, guidance and patience in and outside the project. I am also thankful to Professor Jung-Hoon Chun, who always provided new and challenging ideas for my project.

I would also like to thank Dr. Harold Larson for his help and counsel throughout the duration of the project. I want to thank Dr. Gerardo Trápaga for his advise and counseling on personal matters and for those long and helpful discussions on the project. Thanks to Andrew Gallant from the Central Machine Shop.

I also want to thank the people in the Welding group. Thanks to Don Galler for his advise and help on keeping my equipment running. Thanks to Neil Jenkins, John Matz, Patricio Méndez, Jin-Woo Park and Mikal Balmforth for their friendship.

I would also like to thank all my friends, specially Ante Salcedo, Julio Castrillón, Jorge Carretero and Marcos Escobar to whom I owe my sanity. Thanks to my friend, cousin and roommate Raymundo Arróyave for his advise, support and constant encouragement, specially during the last stages of my thesis work.

Thanks to GALVAK, S.A. de C.V. and the Consejo Nacional de Ciencia y Tecnología in my beloved country, México, for their financial support.

Last but not least, I am truly blessed with my loving parents, brother and sisters. Thank you Mom and Dad, Raúl, Antonieta and Alejandra for your unconditional love and support. Thank you Cecilia for your constant support and your love. I love you all very much.

Table of Contents

List of Figures

List of Tables

Chapter 1 Introduction

1.1 Background

Over the past two decades, metal powder use has increased due to new technologies and applications. The principal rise in metal powder utilization appeared with the advent of powder metallurgy as a near net shape manufacturing process for metallic components, and as an alternative to the conventional production technologies of melting, casting and machining.

Furthermore, with the development of new technologies for producing metal parts and near net shapes, such as powder injection molding and spray forming processes, the use of metallic powders has risen even more. However, some of these technologies require spherical metallic powders as the raw material, and some other uses, such as magneto-rheological fluids, require this particle shape as well.

Consequently, a number of powder production techniques have been developed and optimized in order to fulfill the increasing demands of powder quality. These techniques allow manufacture of a wide spectrum of metal powders designed to meet a variety of applications. Powders of virtually all metals can be produced. Various processes allow precise control of the chemical composition and physical characteristics of powders suitable for specific applications.

As emerging applications appear, new processes or innovations to existing methods arise to meet the quality, cost and performance requirements of these new applications. Hereinafter, a brief discussion of some of the standard technologies and some newer technologies for the production of iron powder will be presented [1].

1.2 Fabrication technologies for iron powder

Iron powder is used in multiple applications such as powder metallurgy, welding rods, flame cutting, food enrichment, and other electronic, magnetic and chemical applications. Powder metallurgy uses the greatest quantity of iron powder, as only one third of the total iron powder produced is used in applications other than powder metallurgy.

There are many technologies for the production of iron powder, which, depending on the nature of the process can be broadly classified as mechanical processes and chemical processes. The most common processes use water and gas atomization, milling, mechanical alloying, electrolysis and chemical methods including reduction of oxides.

1.2.1 Oxide Reduction

The oldest of these methods is the Höeganäs process. This process was developed in Höeganäs, Sweden, and consists of the reduction of iron oxide, in particular, the reduction of iron ore by carbon. Although this process was intended to produce metallic iron in sponge form as the raw material for steelmaking, it proved very useful for the production of iron powder. The use of iron powder produced by this method is limited because of the content of impurities and poor physical and mechanical properties, such as particle size and distribution, particle shape and internal porosity.

The Pyron process is an alternative method to produce iron powder by oxide reduction. In contrast with the Höeganäs process that uses ground iron ore, the Pyron process uses mill scale taken from steel mills that make plain carbon steel products. In this process, the scale is magnetically cleaned and ground in a continuous ball milling operation. This milling ensures the desired particle size distribution. After the milling stage is complete, the material is oxidized to convert the oxides present in the mill scale, FeO and Fe_3O_4, to ferric oxide (Fe_2O_3) which is later reduced by hydrogen in electric furnaces to convert it to iron:

$$Fe_2O_3 + 3H_2 \rightarrow 2Fe + 3H_2O \qquad (1.1)$$

Pyron iron powder has fine porosity and a sponge-like microstructure. It also has an irregular shape.

A third type of oxide reduction process is the Fluidized Bed process. Some variations of this process include fluidized-bed combustion, gasification, heat treatment and catalytic reactions. Fluidized-bed reduction was primarily used in the decade of 1960. Thereafter, electrolytic decomposition, atomization, the carbonyl process and oxide reduction processes replaced this process.

In the fluidized-bed, a granular material is kept in fluid motion using a fluidizing gas, which reacts chemically with the granular solid. In the case of fluidized-bed oxidation, the gas typically is air or oxygen. On the other hand, in the fluidized-bed reduction, the fluidizing gas contains hydrogen or carbon monoxide, or a mixture of the two.

1.2.2 Atomization

Atomization processes are widely used for making both iron and steel powders. This process consists of mechanical disintegration of a molten metal stream into small droplets that are rapidly cooled by means of conductive and/or convective heat transfer.

The atomization process can be sub-classified depending on the atomization medium, as it can either be done by using inert gas, oil or water as the atomization medium [2]. Other modified versions of atomization are centrifugal, vacuum, ultrasonic and rotating disk atomization.

The water, oil and gas atomization processes consist of hitting a molten stream of liquid metal with a jet of gas or water to break it into small particles. When gas breaks up the

molten stream, the cooling rate is lower, allowing surface tension to re-shape the resulting droplets into spherical particles before they solidify [3].

Inert gas atomization is the leading process for the production of high-grade metal powders whose specific quality criteria are spherical particle shape, high bulk density and flowability as well as high purity with low oxygen content. On the other hand, water atomization yields irregularly shaped particles due to a higher cooling rate, although it is also very widely used in industry due to a larger production rate and lower costs than the gas atomizing process.

One variant of the atomization processes, the impact atomization process, consists of breaking up the stream of molten metal by mechanical means, usually a palette rotating at very high speeds. These blades break the stream into very small droplets that are thrown into a falling stream of water, solidifying them on contact [4]. The cooling process can vary to accommodate different cooling rates and control the final shape of the particles.

In this process, the final particle shape and size depend on the size of the stream and its velocity, on the stream-breaking mechanism as well as the rotating speed and atomization angles. This mechanism is also a combination of two phenomena, the pure impact mechanism and the centrifugal effect, which are explained to more detail below.

Centrifugal atomization processes are different from these previous processes in the way that they also use a mechanical force to atomize the liquid metal, but in this case the centrifugal force is exerted on the metal in a different manner. The molten metal is poured into a rotating disc with small orifices in the outer diameter. This way, the melt is driven to the outer surface of the disc and is forced out of the disc through these orifices to cool down while falling into a collector system or to an outer cup containing a cooling liquid [5]. These processes can vary in terms of cooling mechanisms and equipment layout, but the essence of the process is the one described above.

Ultrasonic atomization processes use high frequency vibration to break a molten stream of metal into fine particles. These vibrations can be imposed by either mechanical or electromagnetic means. In the case of mechanical methods, the primary mechanism of break-up is imposing high frequency vibration on the melt stream at the moment it is exiting the crucible where the material is being melted. This operation can be done with a piezoelectric crystal by alternating the electric signal applied to the crystal. The piezoelectric will transmit its vibration to an attached mechanism that imposes the same vibration to the melt and to the melt stream breaking it up into small particles.

Processes such as spray forming have been optimized using this principle, allowing for uniform particle size distribution by controlling both the vibrating frequency and the exit orifice of the melt [6].

Another example is a variation of the Plasma Rotating Electrode Process (PREP), usually applied to produce particles larger than 80μm in diameter. In centrifugal atomization, the usual configuration both in laboratory and large scale industrial practice is the PREP process, used to melt a cylindrical rod using a stationary electric arc while the rod is rotated at high speeds of 10,000 to 20,000 r.p.m. Even though this process is effective, the facility needs a special high speed driving motor and supporting mechanics for the rotating components, which are disadvantageous from a cost-benefit perspective.

A variation of this process is to use the same equipment configuration except for the rotation of the bar. Instead of bring rotated, the bar is attached to a vibrating mechanism at ultrasonic frequency which causes the molten material on top of the bar to form capillary waves and to be atomized into droplets. Other variations of this technique exist, but the principle remains the same: atomization through vibrations.

Recently, some newer techniques that combine other melting mechanisms with atomization techniques have been developed. Two examples of new methods are Plasma

Melting in combination with Gas Atomization and Electrode Induction Melting in combination with Gas Atomization.

In the Plasma Melting process, the material is melted in a water-cooled metallic crucible with plasma heat sources to avoid any contamination of the particles by contact with ceramic crucibles. Once the material is molten, it is atomized with inert gas, assuring minimum contamination of the particles [7]. This process, as well as the Electrode Induction Melting process, yields superclean materials.

The Electrode Induction Melting process also avoids contamination due to contact with liner ceramics. A vertical rotating electrode is continuously melted at the front-end section; therefore the electrode is dipped into a specially design coil [7]. Through an automatic control system of the feeding speed, the melting power and the subsequent atomization setup, a continuous atomization is possible. Atomization is done by inert gas atomization.

1.2.3 Chemical Decomposition

Very fine iron powders can be produced by carbonyl decomposition [8]. This process yields ultra fine spherical particles ranging from 1 to 10 μm in diameter. The starting raw material for the production of iron micropowders is a relatively coarse iron. The iron is exposed to carbon monoxide at high pressure and moderately elevated temperature. The gas reacts with the iron according to the reaction

$$Fe + 5CO \rightarrow Fe(CO)_5 \qquad (1.2)$$

to produce gaseous iron pentacarbonyl. This gas is later condensed to a liquid and reduced under pressure in such a way that it vaporizes again and passes through a decomposer where it is mixed with a small amount of ammonia (NH_3). The decomposer

is externally heated, causing the iron pentacarbonyl to decompose back into iron and CO gas.

Various grades of powder can be manufactured for applications as varied as radar absorbing materials, electronic cores, dietary supplements, and powder metal parts. For some special applications, the resulting powders are reduced by heat treatment in a hydrogen-containing atmosphere to remove carbon and nitrogen, achieving one of the purest forms of iron available.

1.2.4 Electrolytic Iron Powder

Electrolytic iron powder has the highest purity among all types of commercially available iron powders. The process consists of either depositing a loosely adhering, powdery deposit directly onto a permanent cathode or depositing a smooth, dense layer of refined metal on a cathode and subsequently milling to obtain powder. In either case, the resulting particles present irregular shapes. Due to the high cost of manufacture, its usage is limited to specific chemical, catalyst and food-additive applications.

1.3 Motivation and Goals of Research

Although there are many manufacturing processes available today to produce metallic powders, only a few of these processes can be used to produce iron powder. As new applications for iron powder emerge, more stringent requirements have to be met regarding powder properties; such requirements imply both chemical and physical properties including particle shape and size.

To satisfy the industry requirements, new processes are needed to overcome these constantly increasing limitations as alternate processes to the carbonyl process and those atomization processes that yield spherical particle shape at high costs compared to those that yield irregular particles.

A simple technique consisting of melting irregularly shaped particles inside a vertical tube furnace is explored in this thesis. Although this technique has been used in the past to produce single particles, it has not been used to mass-produce spherical iron powder.

The purpose of this work is to extend this technique to mass-production of spherical iron powder from atomized powders. The powders to be processed range in size from 15 to 100 μm in diameter, although larger particle sizes can also be processed. A variation of this process has also been used to produce W-Co agglomerates [9] at higher temperatures than that needed to melt iron with acceptable results.

The basic sketch of the apparatus built in the course of this work is presented in Figure 1.1.

The goal of this research is to develop a better understanding of this technique and its application to process iron or other iron alloy powders. Also, an important part of this research is to understand the physics of the process, mainly the heat transfer mechanisms and the particles' behavior within the furnace, and to characterize the physical parameters that define the system.

1.4 Outline of the Study

While this chapter has provided an introduction to the project and its primary objectives and a brief discussion of available powder manufacturing technologies and their characteristics, the next chapter presents the basic physical models that describe the process along with some predicted results. Chapter Two presents the physical models of particle motion and dispersion as well as the heat transfer mechanisms involved during heating and cooling of the particles. Chapter Three describes the experimental method employed to produce spherical particles including experimental results. Finally, a summary of this thesis and recommendations for future work are given in Chapter Four.

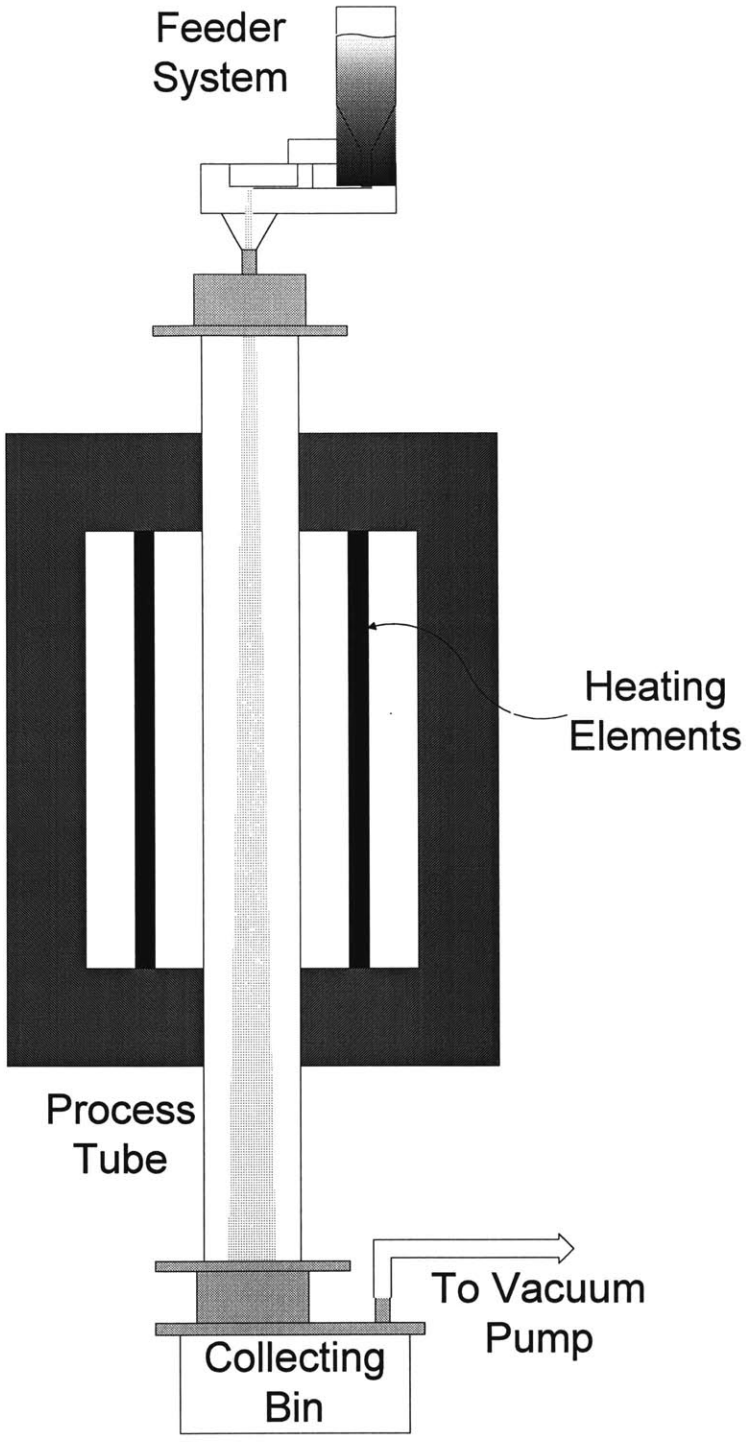

Figure 1.1: Schematic drawing of apparatus used to spheroidize powder.

Chapter 2 Process Description

The proposed process consists of a drop tube heated by electric resistors in which small irregularly shaped iron particles rapidly melt by thermal radiation and form spherical particles by means of surface tension.

The raw material used in the process is water-atomized iron powder. The final particle size is dependent primarily on the initial particle size of the starting material, although it also depends upon processing parameters and equipment dimensions.

Carrying out the process in a vacuum modifies the process and simplifies the analysis from an analytical point of view by eliminating the convective heat transfer effect. When the process is carried out at atmospheric pressure, the critical effect of natural convection must be taken into account. The problem of including convective heat transfer is that at atmospheric pressure and high temperatures, enhanced convective flows should appear inside the tube, invalidating the model of a freely falling sphere. Also, since the small molten particles will not fall through the tube but instead follow these convective flows, they will increase the probability to collide with each other and with the tube walls and the tube may be clogged by the accumulated metal powder.

2.1 Particle Trajectory

2.1.1 Terminal Velocity

Consider the falling particles as spherical flowing through stagnant air at low pressure. When a gas is in the continuum flow regime and at low pressures -- less than 10 atmospheres --, the pressure has no effect on the viscosity of the gas and the viscosity is greatly affected by the gas temperature [10].

The Knudsen Number is used to determine the type of flow regime. This number can be written as the ratio of the mean free path of the molecules, that is, the average distance

the gas molecules have to travel before colliding with another molecule, and the characteristic length of the system. In the case of the system being described here, the characteristic length of the system is the tube diameter. The mean free path can be expressed as a function of the gas pressure, temperature and the molecules' characteristic diameter, σ [11, 12, 13]:

$$\lambda = \frac{\kappa_B T}{P\pi\sigma^2} \qquad (2.1)$$

$$Kn = \frac{\lambda}{D} \qquad (2.2)$$

In these two expressions, λ represents the mean free path, T is the absolute temperature, P is the pressure, κ_B is the Boltzmann constant and σ is the characteristic diameter of the molecule. Kn is the Knudsen Number and D is the tube diameter. The flow regimes are characterized by the magnitude of the Knudsen number [12]. Table 2-1 summarizes these classifications.

Table 2-1 : Flow Regimes

Continuum	$Kn < 10^{-3}$
Slip Flow	$10^{-3} < Kn < 0.25$
Transitional Flow	$0.25 < Kn < 10$
Free Molecular Flow	$Kn > 10$

For air at 1800 K, and 0.1 Atm, the mean free path is of the order of 10^{-7} meters and the Knudsen number for this system is of the order of 10^{-6}, hence the system consists of continuum flow regime. The required pressure for the system to change to slip flow has to be less than 10 Torr and less than 10^{-4} Torr to be in free molecular flow.

The forces acting on the falling particle are the weight of the particle forcing it to fall, the buoyant force exerted by the gas and the drag force acting in the opposite direction of the motion. The effect of these forces appear graphically in Figure 2.1.

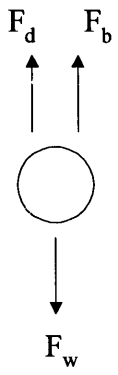

Figure 2.1: Forces acting on a particle

The drag force F_d is related to the particle motion and it is quantified by the drag coefficient, the particle size and the gas properties. The drag coefficient is a function of the shape of the particle and the particle's Reynolds number. Similarly, the buoyant force F_b is the force exerted by the fluid on the particle even when the gas is stationary [10]. These forces can be expressed as:

$$F_w = \rho_p V g \qquad (2.3)$$

$$F_d = \frac{C_d A_p \rho_f U_b^2}{2} \qquad (2.4)$$

$$F_b = V \rho_f g \qquad (2.5)$$

In the above expressions, C_d is the drag coefficient, ρ_f is the gas density, A_p is the projected area of the particle, U_b is the bulk velocity relative to the particle, V is the particle volume and g is the gravitational acceleration constant.

Assuming spherical particle shape, these formulas can be simplified for this specific geometry. The drag coefficient C_d is the ratio of the gravitational force to the inertial force. For spherical particles it can be written as equation (2.6) for creeping flow conditions and as equation (2.7) in the intermediate region before Newton's Law region. Newton's Law of viscosity states that the shear stress between adjacent fluid layers is proportional to the negative value of the velocity gradient. This last regime is characterized by Reynolds numbers greater than approximately 500, and the drag coefficient for spheres has a constant value of 0.44 in this region.

$$C_d = \frac{24}{\mathrm{Re}_p} \qquad \mathrm{Re}_p < 2 \qquad (2.6)$$

$$C_d = \frac{18.5}{\mathrm{Re}_p^{0.6}} \qquad 2 \leq \mathrm{Re} \leq 500 \qquad (2.7)$$

The particle's Reynolds number is a function of the particle diameter, d_p, the gas velocity relative to that of the particle, U_b, the fluid density, ρ_f, and the gas viscosity μ:

$$\mathrm{Re}_p = \frac{d_p U_b \rho_f}{\mu} \qquad (2.8)$$

For low pressures under continuum flow, the viscosity of a gas is independent of the pressure and depends only on temperature. Using the Lennard-Jones potential, Chapman and Enskog [10] developed the following equation for the viscosity of a non-polar gas at low pressures (<10 atm):

$$\mu = 2.67 \times 10^{-5} \frac{\sqrt{MT}}{\sigma^2 \Omega n} \qquad (2.9)$$

where μ is the dynamic viscosity in poises; M is the gram-molecular weight of the gas; σ is the characteristic diameter of the molecule in Angstroms; T is the absolute temperature of the gas and Ωn is the collision integral of the Chapman-Enskog theory. Values for the collision integral Ωn are extensively tabulated; its value is independent of pressure and depends only on the dimensionless temperature parameter $\kappa_B T/\epsilon$, where ϵ is the characteristic energy parameter and κ_B is the Boltzmann constant. For air at 0.1 atmosphere and an absolute temperature of 1800 K, the calculated values for Ωn and σ are 0.73 and 3.711 Å respectively [10].

Under creeping flow conditions, equations (2.4) and (2.5) can be rearranged for a spherical particle as

$$F_d = 3\pi d_p U_b \mu \qquad (2.10)$$

$$F_b = \frac{\pi}{6} d_p^3 \rho g \qquad (2.11)$$

Under creeping flow conditions, Stokes' Law -- equation (2.10) -- is used to calculate the particles' terminal velocity by setting the relative velocity U_b to the final velocity V_f and solving for the final velocity, thus providing the system of forces acting on the particle. The resulting equation for the final velocity is

$$V_f = \frac{d_p^2 g(\rho_p - \rho_f)}{18\mu} \qquad (2.12)$$

This equation holds for Reynolds Numbers less than approximately one. The above equation states that the final velocity a particle can reach, depends on particle size as well

as the fluid density and viscosity, which are functions of pressure and temperature respectively. Also, for small feed rates, the spacing between particles is larger than 2 particle diameters, therefore, no interactions between particles can be assumed and no adjustment of the drag coefficient is necessary. This effect is verified experimentally later in Chapter Three.

2.1.2 Initial Velocity and Residence Time

Since the viscosity increases with temperature, the drag force also increases with increasing temperatures. We can also anticipate increases in drag as the particle size decreases, therefore the terminal velocity will increase as the particle size increases. Furthermore, for very small particles, the drag force is notably large and the corresponding terminal velocity will be very small due to the large specific area of the small particles. The effect of particle diameter and temperature on the terminal velocity can be seen graphically in Figure 2.2.

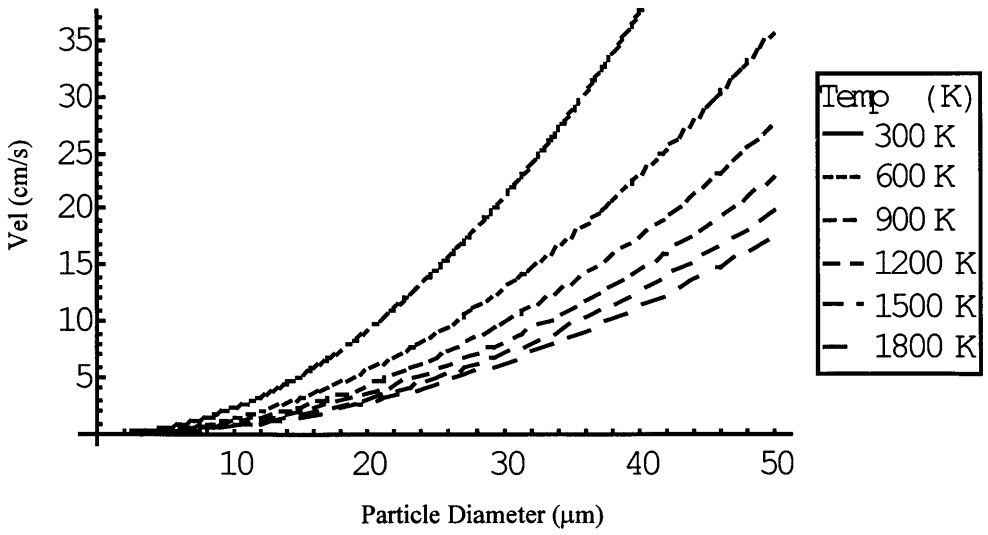

Figure 2.2: Particle terminal velocity as a function of particle size at 0.1 Atm

As the particles begin to fall, they accelerate gradually until they reach the terminal velocity. For small particles, the time necessary to reach the terminal velocity is very small. Following the same approach used to calculate the terminal velocity we can calculate the effective acceleration of the particle, a:

$$a = \frac{d_p^2 g(\rho_p - \rho_f) - 18 U_b \mu_f}{d_p^2 \rho_f} \qquad (2.13)$$

Solving the above equation iteratively with the free fall velocity and travel distance equations, we obtain different curves for the particles' velocity as a function of time for various particle sizes. These curves are displayed in Figure 2.3 and Figure 2.4. Note that for smaller particles, the particles attain their final velocity almost instantly and consequently they will travel at their final velocity throughout the process.

Since the velocity is constant for small particles, the residence time will also behave linearly with the flight distance. Figure 2.5 shows the estimated residence time for different particle sizes as a function of flight distance, assuming the particles reach their terminal velocity instantaneously.

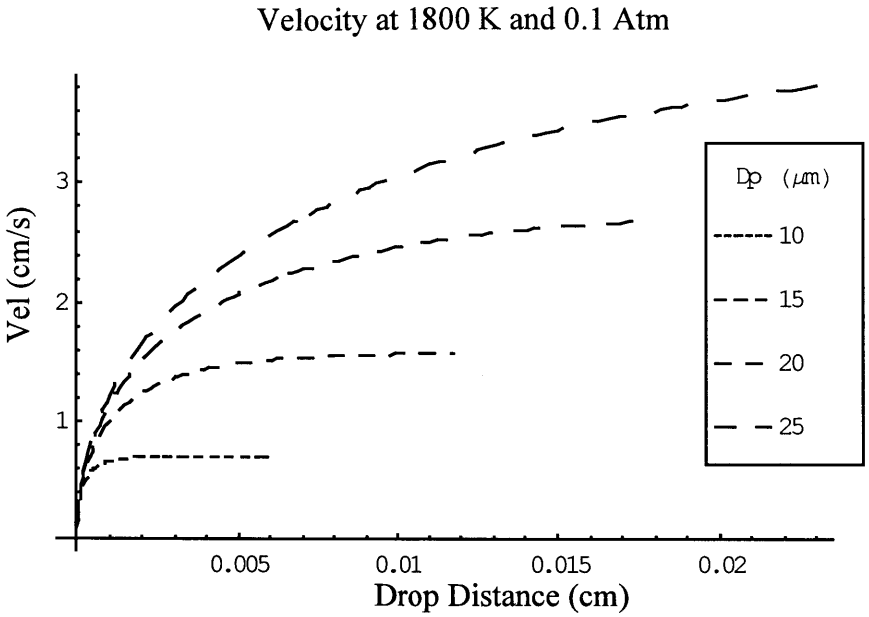

Figure 2.3: Initial velocity for small particles as a function of travel distance

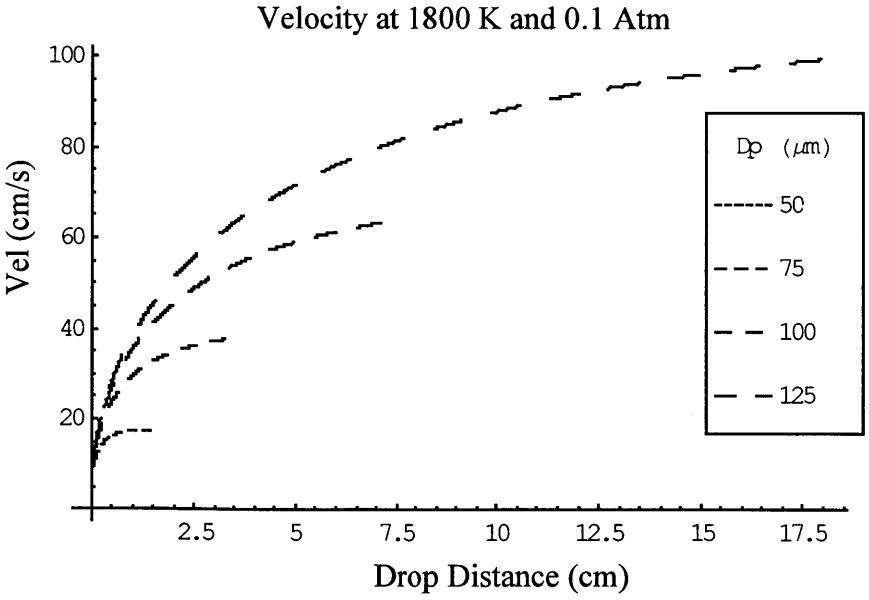

Figure 2.4: Initial velocity for large particles as a function of travel distance

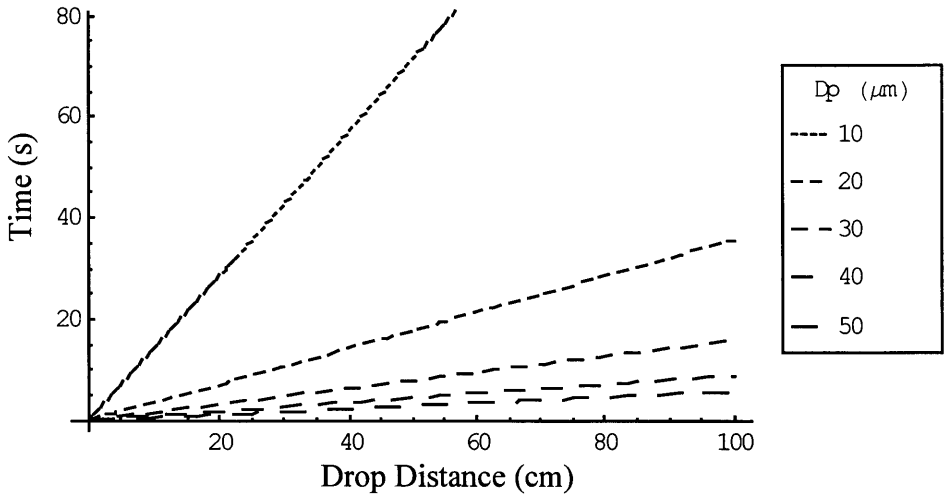

Figure 2.5: Particle flight time vs. tube length in air at 0.1 Atm and 1800 K

2.2 Particle Heat Transfer Model

For small spherical particles, we can assume Newtonian heating and cooling when the Biot number is less than 0.1, that is, no internal gradients of temperature exist within the particle. For small iron particles, the Biot number is in the order of 10^{-3}. These values were calculated using the characteristic length of the particle, and the total heat transfer coefficient, h_t. For spherical particles, the characteristic length is the particles' diameter. The total heat transfer coefficient is the sum of both the convective and radiative heat transfer coefficients.

Since the system is operating in vacuum, the convective heat transfer coefficient h_c is negligible compared to the radiative heat transfer coefficient h_r, therefore the total heat transfer coefficient can be assumed to indicate only radiative heat transfer (see Table 2-2). This radiative coefficient is derived from the total heat transfer to the particle and can be written as equation (2.15) [10]:

$$h_t = h_c + h_r \tag{2.14}$$

$$h_r = \mathcal{F}\sigma\left(\frac{T_p^4 - T_\infty^4}{T_p - T_\infty}\right) \tag{2.15}$$

Where $\mathcal{F}$ is the view factor between the particle and the surrounding areas. The view factor encompasses the geometric configuration factor and the emissivity. In the case when the particle is completely surrounded by a large surface with constant temperature T_∞ the view factor $\mathcal{F}$ reduces to ε, the emissivity of the particle. A comparison of the radiative and convective heat transfer coefficients is shown in Table 2-2.

Table 2-2: Comparison of heat transfer coefficients at 1800 K

Pressure	0.1 Atm	0.4 Atm	0.7 Atm	1.0 Atm
hc (W/m^2-k)	2.14	3.03	3.64	4.14
hr (W/m^2-k)	896	896	896	896

The particles' Biot number depends also on the thermal conductivity, k, and is given by

$$Bi = \frac{h_r d_p}{k} \tag{2.16}$$

When the interaction between particles is important, the effective emissivity of the particles has to be corrected for the emissivity of a cloud of particles, which absorbs part of the radiation and hinders the total radiative heat transfer to the particles. The emissivity for a cloud of particles, ε_c, is shown in equation (2.17).

$$\varepsilon_c = 1 - \exp(-\varepsilon_p N_p L A_p) \qquad (2.17)$$

where ε_p is the particles' emissivity, N_p is the concentration of particles per unit volume, L is the length of the cloud of particles and A_p is the average cross-sectional area of the particles [14]. We may assume that the particles do not spread in their trajectory as the limiting case and that they remain uniformly distributed throughout their whole flight time with a distribution equal to the initial spreading across the inlet area.

Setting the length of the cloud as the distance L, we can rewrite the above equation as a function of physical parameters of the system such as feed rate, inlet diameter and particle diameter. In SI units:

$$\varepsilon_c = 1\text{-}\exp\left(\frac{-10 8 \varepsilon_p \mu_f FeedRate L}{d_p^3 g \rho_p^2 d_{inlet}^2 \pi}\right) \qquad (2.18)$$

For small particles and low feed rates, the ε_c is of the order of 10^{-4}, hence the cloud of particles has no effect on the particle emissivity and no correction is needed.

Having calculated the Biot number and determined the Newtonian conditions, the controlling differential equation for heating and cooling is based on a heat transfer balance to or from the particle:

$$q = \dot{m} C_p \frac{dT}{dt} = h_t A (T - T_\infty) = \varepsilon \sigma A (T^4 - T_\infty^4) \qquad (2.19)$$

$$\frac{dT}{dt} = (T^4 - T_\infty^4)\left[\frac{6\varepsilon\sigma}{\rho_p C_p d_p}\right] \qquad (2.20)$$

In the above equations, σ is the Stefan-Boltzmann constant, A is the surface area of the particle and C_p is the specific heat of the material at constant pressure.

Integrating equation (2.20) using partial fractions and solving for the limits of integration yields equation (2.21), that holds for both heating and cooling. This equation can also be used to calculate the superheating in the particle once the particle melts, using the specific heat of the liquid phase instead of that of the solid phase.

$$\frac{6\varepsilon\sigma(t - t_0)}{\rho_p C_p d_p} = \frac{1}{2T_\infty^3}\left[Tan^{-1}\left(\frac{T}{T_\infty}\right) - Tan^{-1}\left(\frac{T_0}{T_\infty}\right)\right] + \frac{1}{4T_\infty^3}\left\{\left[Ln(T_\infty + T) - Ln(T_\infty + T_0)\right] - \left[Ln(T - T_\infty) - Ln(T_0 - T_\infty)\right]\right\} \quad (2.21)$$

A simple heat balance calculation yields the time needed to melt the particles once they reach their melting point. Using the effective specific heat of the material in the above equation and the appropriate temperature range, one can obtain the melting time. The effective specific heat adds to the specific heat of the solid phase the latent heat of fusion divided by the temperature range in which the material completes the phase change from solid to liquid or vice versa. The results of the heat transfer modeling can be summarized in Figures 2.6 to 2.8. Figure 2.6 shows the required travel distance to melt the particles at 0.1 Atm and various drop tube temperatures. This plot shows values for iron particles with melting point of 1535 C.

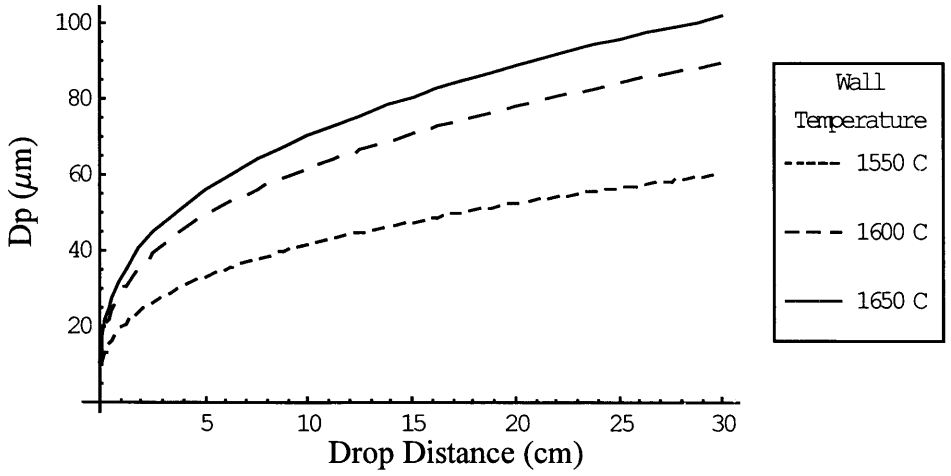

Figure 2.6: Required Distance to Melt Iron Powder

The results from Figure 2.6 are in agreement with the experimental results. These results will be discussed later in Chapter Three.

A model of how the particle heats up, melts and solidifies as it passes through each of the cold and hot zones of the furnace can be constructed by solving equation (2.21) for each zone in the furnace. Results of this model are shown in Figure 2.7 and Figure 2.8.

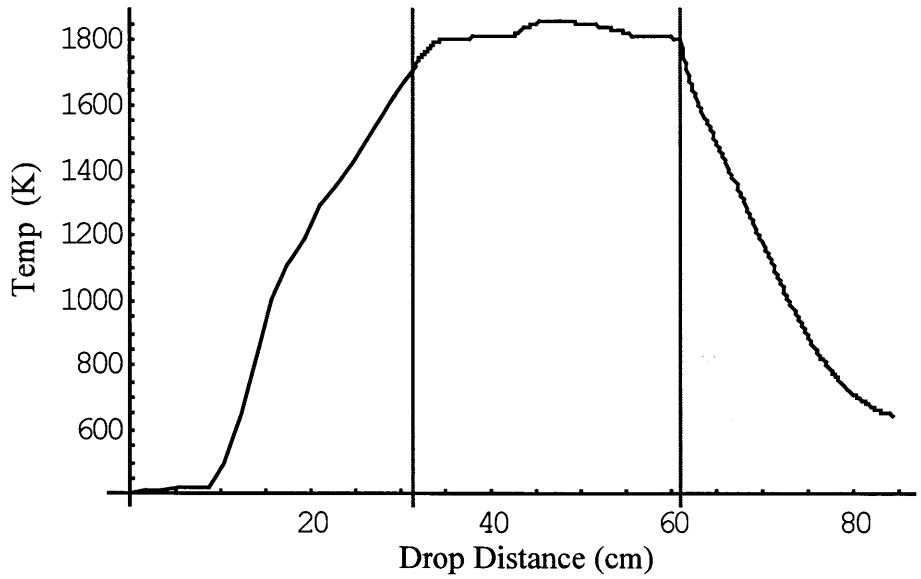

Figure 2.7: Particle Temperature vs. Drop Distance
Operating Pressure: 0.1 Atm; Particle Diameter: 50μm

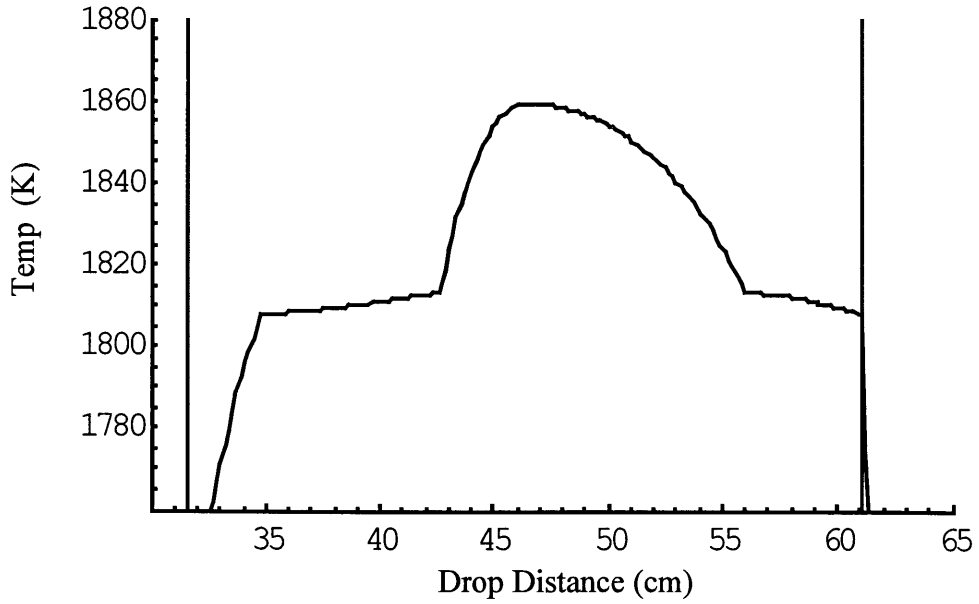

Figure 2.8: Particle Temperature vs. Drop Distance
Operating Pressure: 0.1 Atm; Particle Diameter: 50μm

These two figures are delimited by two vertical lines that indicate the change of zone within the furnace. In the first zone, the pre-heating zone, the particles heat up to the tube wall temperature, which rises at a nearly linear rate to the melting zone temperature. This pre-heating zone can be as short as needed, since the heating time needed to raise the particles' temperature to the melting point is negligible compared to the time required for melting the particle. The complete mathematical model used to obtain these plots is shown in Appendix A. This model uses experimental values of the tube temperature profile to calculate the particles' temperature at a given distance.

Figure 2.8 focuses on the particles' temperature in the middle zone or melting zone. In the first part of this plot, the particle remains at the melting temperature while melting takes place. After melting is completed, the molten particle suddenly raises its temperature to approximately that of the tube wall temperature until it reaches its peak value. From that point forward, the particle starts to cool down following the tube temperature profile until it reaches the melting temperature, where it starts to solidify. Once solidification is completed, the particle cools down in the last zone, the cooling zone, following once again the tube temperature profile. The required distance to melt for a 50 μm particle in Figure 2.6 corresponds to what is shown in Figure 2.8.

Chapter 3 Experimental Apparatus and Procedure

3.1 Equipment Description

Figure 1.1 shows a schematic of the apparatus utilized to spheroidize the powder. The equipment consists of a tube furnace lined up with a dense alumina cylinder eight inches inside diameter and one inch thick as a first insulating layer backed up with a layer of porous alumina firebrick (2800 F) two inches thick. This same configuration was used on top and bottom of the furnace during construction.

The furnace has four 0.5" openings to accommodate four silicon carbide heating elements rated at 2Ω of electrical resistance each. They are symmetrically arranged at a radius of 3" from the furnace center. The center opening accommodates an alumina tube of 3" diameter and 3 foot long. The heating elements can raise the temperature of the furnace to 1650 C, although normal operating temperature is 1600C. This temperature is measured outside the process tube in the hot chamber of the furnace and is controlled by a closed-loop control system. The furnace operates at 220 VAC, 1Φ, 20A.

Since the system operates in vacuum, a feeder system was designed and built to allow constant and steady feed rates to the furnace. The feeder operation consists of a hopper feeding powder by gravity to a rotating disc; the disc is rotating at a fixed speed of 1 r.p.m. The powder travels on the disc to the opposite side of the feeder where it is pushed off of the disc and into a funnel by a sweeping blade. The discharge of the funnel connects directly to the process tube inlet. A section view of the feeder system can be seen in Figure 3.1.

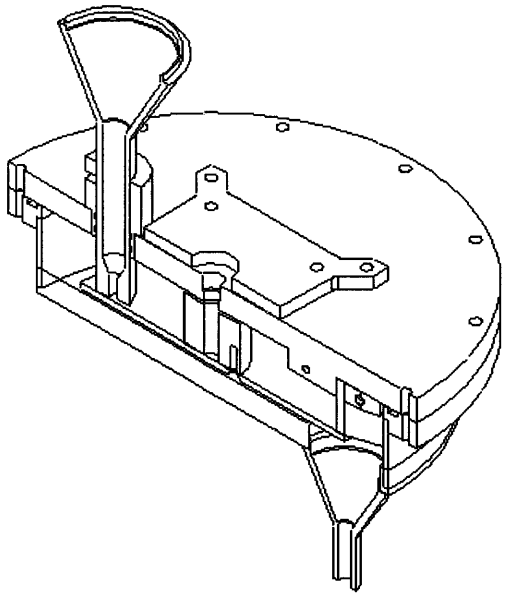

Figure 3.1: Cross section view of feeder system

The processed particles are collected at the bottom of the drop tube in a stainless steel bin that is emptied after a complete batch of material has been processed. This collecting bin is attached to a brass structure that connects to the bottom of the process tube. The vacuum pump connects to this unit.

The vacuum system is comprised of a positive-displacement rotary piston mechanical pump, an air filter and a heat exchanger to cool the air going into the pump. This heat exchanger is necessary to operate the pump for long periods of time, and avoid possible overheating of the pump.

3.2 Challenges in Spheroidization

Initial attempts to spheroidize iron powder were made in a process tube of 2" diameter at atmospheric pressures by manually feeding the material into the furnace. Because of the high temperatures within the alumina tube, convective flows are induced and carry the particles away from their free fall trajectory impacting them with the tube wall.

Complete spheroidization was achieved under these conditions, for small batches of 20 to 40 grams of material, although approximately half of the material was lost to the tube walls. Similarly, when attempting to process larger batches of material with an automatic feeding system, the convective flows within the process tube impacted the particles with the walls, resulting in complete clogging of the process tube with metal powder after a few grams of material had been processed.

This behavior is mitigated as the particle size increases since the particle weight is large relative to the convective flow force and thus the particle is large enough for it to continue on its free fall trajectory. The obvious solution to the problem of convective flows with small particles was to eliminate the convective flows by adapting the equipment to process the material in a vacuum.

New limitations arise by processing the material in a vacuum. The convective heat transfer component decreases substantially and the heat transfer will then be radiation controlled. Considering the strong dependence of these new process conditions on particle size and the materials radiative properties shown in Chapter Two, there is a tradeoff between the operating pressure and the maximum particle size that can be processed when reducing the pressure.

3.3 Experimental Procedure

3.3.1 Material Preparation

Powder samples were obtained from three different suppliers. Before proceeding to process the received powder, a smaller sample was separated and sieved to test for particle size distribution. This procedure was done in accordance with both ASTM Standard B214 [15] and MPIF Standard 05 [16]. If the sample had a large amount of coarse particles, all the material to be processed was sieved and only those particles with particle size smaller than standard mesh size 325 (45 μm) were actually processed. On the other hand, if the material had a small amount of coarse particles, the material was processed directly with no further separation.

3.3.2 Equipment Setup

Before each experiment, the collecting bin and the feeder system were secured in place and the vacuum system tested for leaks. A vacuum reading of 0.15 atm or lower was an acceptable reading to begin processing material. The furnace was turned on until an acceptable vacuum level was achieved.

After processing the material and shutting down the equipment, the collecting bin was left in the equipment to cool down. Once the material cooled down to room temperature, the powder was collected and analyzed in the same manner as the starting material to characterize particle size distribution. Following the particle size analysis, a sample of the processed material was analyzed for particle shape using a Scanning Electron Microscope (SEM).

3.4 Experimental Results

The results presented herein will emphasize the outcome of the experiments with two different iron powder products. Both samples are water atomized powder, and both were fully sieved for particle size smaller than standard mesh size 325 prior to processing. The first sample is the Atomet® HP-1001 Iron Powder from Quebec Metal Powders. The second sample is the ATW-230® Iron Powder from Höeganäs Corporation. The results from the experiments are reported in the following subsections.

3.4.1 Particle Shape Analysis

The following SEM pictures present a comparison of particle shape before and after processing for each of the two powders mentioned above. These pictures clearly present the capability of this process to completely spheroidize the water-atomized powders. The ovaling effect seen in the set of pictures for the Atomet® powder is due to the method used to take the SEM pictures. A different method that corrected for this photographic effect was used for the ATW-230® SEM pictures.

Figure 3.2 and Figure 3.4 show the shape of a typical water atomized powder. Note that the particle size in the first sample is rather large and therefore was not processed but is shown here to illustrate the typical shape of the starting material. Contrasting with the former two pictures, Figure 3.3 and Figure 3.5 show the perfectly spherical shape of the resulting powder after processing.

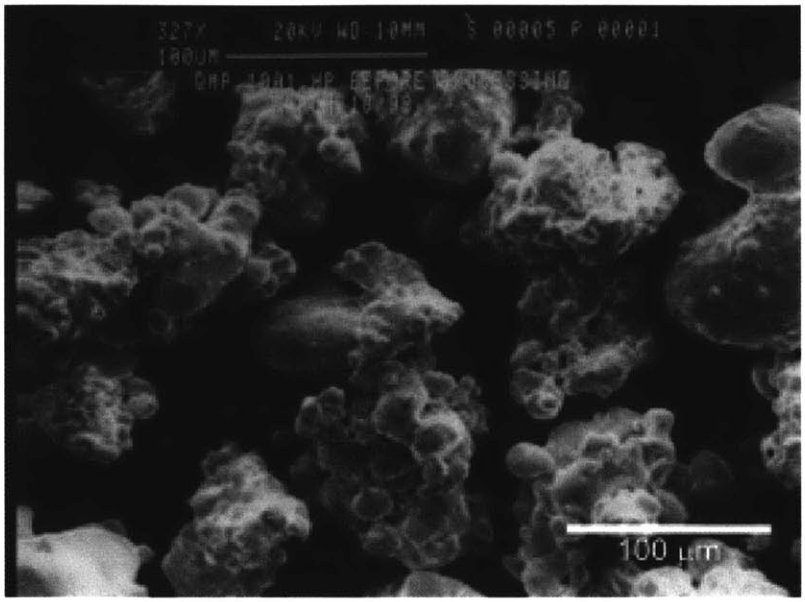

Figure 3.2: Atomet® Iron powder before processing

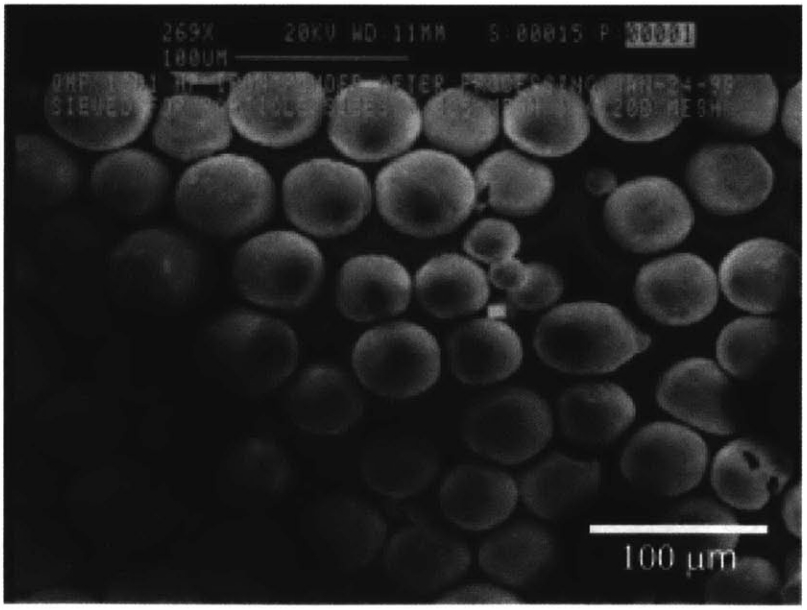

Figure 3.3: Atomet® Iron powder after processing at 80 gr/hr Feed Rate

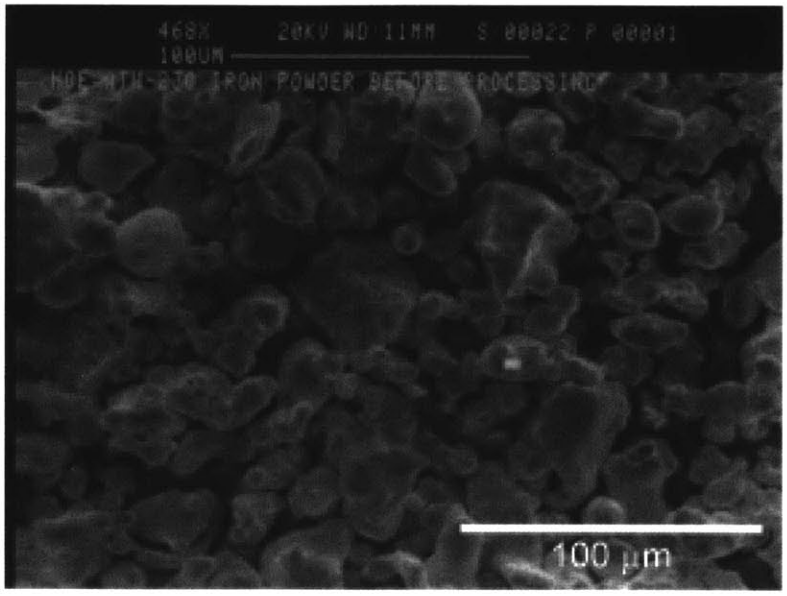

Figure 3.4: ATW-230® Iron Powder Before Processing

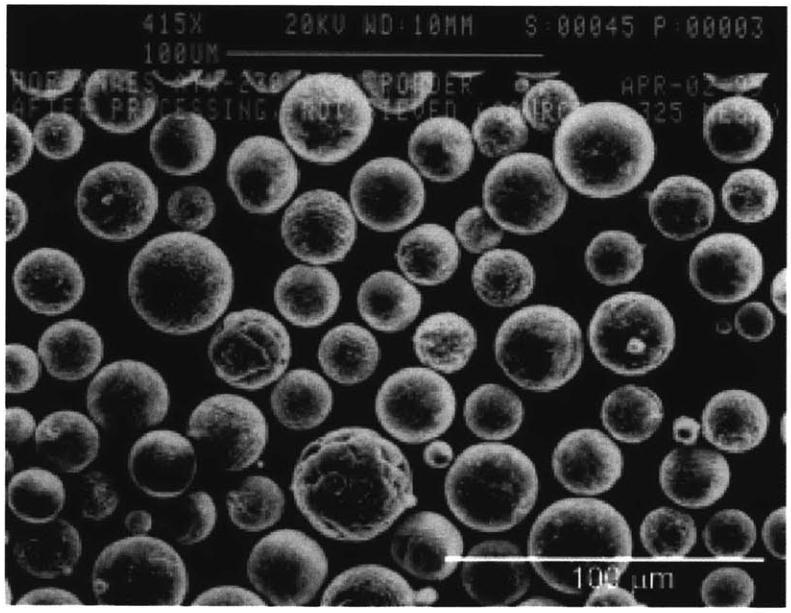

Figure 3.5: ATW-230® Iron Powder After Processing at 100 gr/hr Feed Rate

3.4.2 Particle Size Distribution

Similarly as with the previous comparison for particle shape, the size distribution was obtained from different samples before and after processing. The size distribution was obtained from the SEM pictures using Martin's diameter [1], that is, the length of a line that bisects the area of the particle image.

Figure 3.6 (b) and (c) compares the size distribution for Atomet® Iron Powder. These charts show that for lower feed rates the distribution remains unchanged from the starting size distribution, validating the assumption of no interaction between particles. Although for (c) there is a small change in size distribution, it is still negligible and not sufficient to invalidate the model assumptions.

Analogously, Figure 3.7 (a) and (b) compare the size distribution for ATW-230® Iron powder. The size distribution is almost identical from (a) to (b), however, for feed rates starting at 150 gr/hr a more prominent change in diameter was observed.

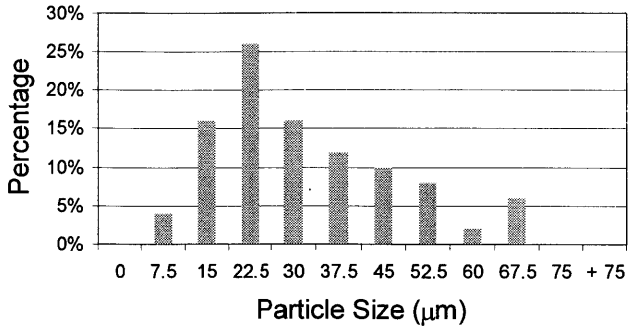

(a) Before Processing

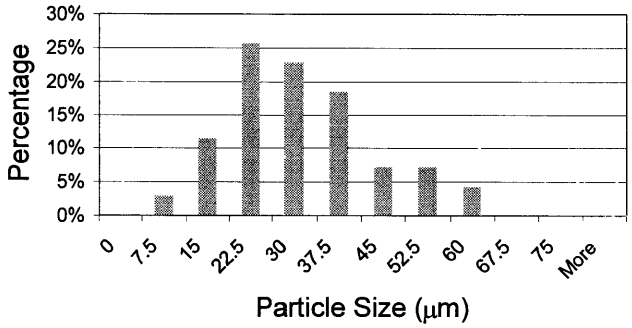

(b) After Processing at 70 gr/hr Feed Rate

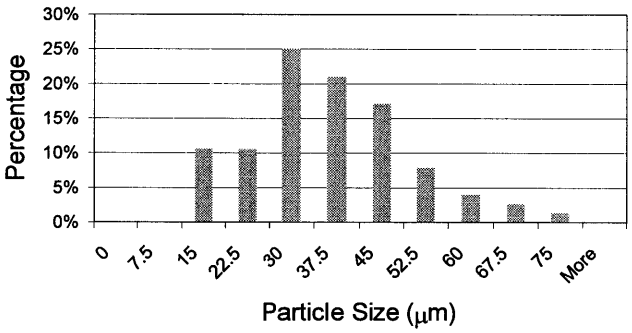

(c) After Processing at 120 gr/hr Feed Rate

Figure 3.6: Particle size distribution for Atomet® Iron Powder

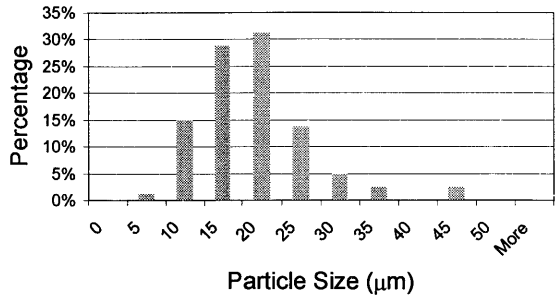

(a) Before Processing

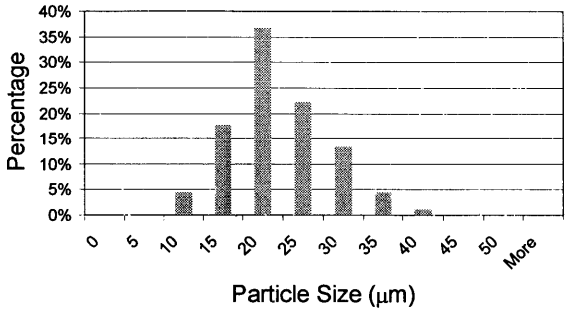

(b) After Processing at 100 gr/hr Feed Rate

Figure 3.7: Particle size Distribution for ATW-230® Iron Powder

3.5 Experimental Validation of the model

Equation (2.21) shows a strong dependency on thermal properties of the material such as specific heat and emissivity. Materials with high emissivity are easier to melt than materials with lower emissivity values. This is the case of stainless steel, which has a low emissivity and was difficult to melt. Also, the effective specific heat of stainless steel is higher than that of pure iron, hence longer residence times are needed to melt stainless steel particles compared to similar sized iron particles.

Analogous to Figure 2.6, Figure 3.8 shows the required distance to melt stainless steel powder. Note that because of the lower emissivity of the stainless steel compared to that of the iron powder, there is a lower limit on the particle size that can be melted with the same configuration as before.

This predicted result was in accordance with the experimental observations, where only partial spheroidization could be achieved when processing stainless steel with the same operating conditions and equipment configuration as used when processing iron powder.

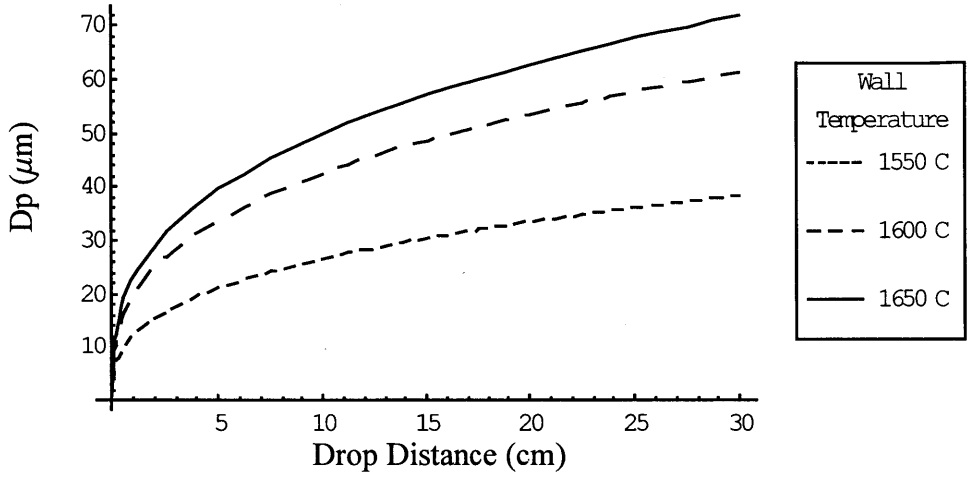

Figure 3.8: Required Distance to Melt Stainless Steel

Chapter 4 Summary

The drop tower process proposed in this study proved to be a viable option to manufacture spherical iron powder. Laboratory tests proved this process successful to spheroidize irregularly shaped particles at low feed rates. However, given the characteristics of the process and the heat requirements of the spheroidization phenomenon, this process can be easily adapted to produce larger quantities of material without a significant change in the equipment configuration. Furthermore, since the melting zone does not need to be long, smaller furnaces can achieve the desired spheroidization. The current configuration of the equipment allowed production of powders with particle size of up to 100 μm, although larger particle sizes can be melted using this process.

Since this process is carried out under a low vacuum, the heat transfer to the particles is radiation controlled and the process is described by the model proposed in Chapter Two. On the other hand, when the process is carried out in a medium to high vacuum, at pressure levels of 10^{-1} Torr or less, the particle motion will no longer be in the continuum regime: the model proposed in Chapter Two will no longer be valid and new assumptions have to made since the particle motion will be in transitional flow or free molecular flow [12] and corrections to the drag coefficient and the fluid properties are needed. Under free molecular flow, the particle velocity will approach that of ideal free fall velocity and the residence time will be very small, imposing a lower limit on the operating pressure of the system.

Melting of the particles has a strong dependency on radiative properties of the material. To successfully process materials with low emissivity, higher residence times are needed to melt the particles and achieve complete spheroidization. The obvious solution is to increase the melting zone length. A plausible second option to overcome the residence time limitation without increasing the melting zone length is to use higher temperature differences between process temperature and the materials' melting point, resulting in

shorter melting times. The furnace under use in this work is limited to operating temperatures of 1625C, therefore high temperature differences between the furnace wall and the melting point of the iron cannot be achieved.

The current equipment configuration allows feed rates of up to 120 grams per hour before significant agglomeration of the particles occur. higher feed rates can be achieved with better spreading of the powder to be processed across the inlet area. This spreading has to take into account spacing between the particles and the tube walls to avoid any particles hitting the walls. These values can be determined experimentally. Currently, the inlet area is 5% of the tube cross sectional area.

In conclusion, this process proved successful for producing spherical iron powder, and changes in the equipment setup, such as operating temperature, could improve the capacity to spheroidize powders that cannot be processed under the present configuration.

References

[1] Lampman, S. R., Ed., ASM Handbook, Vol. 7: Powder Metal Technologies and Applications, ASM International, 1998, v.7, pp. 33-107, 110-122, 259-273

[2] Lubanska, H. J. of Metals, 1970, v.22, pp.45

[3] Klar, E., Shafer, W.M. "Powder Metallurgy for High Performance Applications", Syracuse University Press, 1972 , p.57

[4] Wanibe, Y., Itoh, T., Matsui, Y., "Impact Atomization of Liquid Metals", The International Journal of Powder Metallurgy, 1991, v.27, n.3, pp. 195-208

[5] Cooper, K.P., Ayers, J.D., "Counter Rotating Fluid Atomization", The International Journal of Powder Metallurgy, 1993, v.29, n.3, pp. 215-226

[6] Chen, C., "Droplet Solidification and its Effects on Deposit Microstructure in the Uniform Droplet Spray Process", Ph.D. Thesis, Department of Mechanical Engineering, MIT, 1996

[7] Hohmann, M., Ertl, M., "New Technologies for the Production of High Grade Metal Powder", Advances in Powder Metallurgy, APMI, MPIF, Leybold, A.G. Ed, 1990, v.1, pp.37-48

[8] Japke, J.E. "Iron Powder for Metal Injection Molding" The International Journal of Powder Metallurgy, 1991, v.27, n.2, pp. 107-114

[9] Tremblay, S.P., Angers, R.H., "Spheroidization of WC-Co Agglomerates", The International Journal of Powder Metallurgy, 1989, v.25, n.3, pp.179-184

[10] Poirier, D.R., Geiger, G.H., Transport Phenomena in Materials Processing, The Minerals, Metals and Materials Society, 1994, pp. 3-13, 68-71

[11] Holland, L., Steckelmacher, W., Yarwood, J., Vacuum Manual, E.& F. N. SPON, 1974, pp. 15-19

[12] Crowe, C., Sommerfeld, M., Tsuji, Y., Multiphase Flows with Droplets and Particles, CRC Press, 1998, pp. 67-80

[13] Burmeister, L., Convective Heat Transfer, John Wiley and Sons, 1983, pp. 33-37

[14] Szekely, J., Themelis, N.J., Rate Phenomena in Process Metallurgy, Wiley Interscience,1971,pp. 299-300

[15] American Society for Testing and Materials, Standard B214,1998

[16] Metal Powder Industries Federation, Standard 05, 1995

[17] Pehlke, R.D., Jeyarajan, A., Wada, H. Summary of Thermal Properties for Casting Alloys and Mold Materials, NTIS, 1982, pp. 3-28, 40-53

[18] Patterson, G.N. Molecular Flow of Gases, John Wiley and Sons, 1956, pp. 1-20, 159-191

AppendixA

Particle Spheroidization Model

Mathematica® V.3.0

```
(* Graphics Modules to be used *)
<< Graphics`MultipleListPlot`
<< Graphics`Graphics`
<< Graphics`Legend`
pagewidth = 400; (* points; 72 points = 1 in. *)
```

■ *Particle Trajectory Model*

General Materials and Input Data

```
tAir = Range[300, 1800, 300]; (* K *)
pAir = Range[.1, 1, .3]; (* Atm *)
gravAccel = 9.81; (* m/s^2 *)
mwAir = 28.97; (* gr-mol *)
rAir = 287; (* m^2/(s^2 K) *)
ρFe = 7800; (* kg/m^3 *)
rUniv = 8.31451; (* J/grmol-K *)
furHotLength = 12 * 0.0254 ; (* m; Length of Hot Zone *)
furColdLength = 12 * 0.0254; (* m; Length of Cold Zone *)
tOper = 1800; (* K *)
pOper = 0.1; (* Atm *)
posT = First[Flatten[Position[tAir, tOper]]];
posP = First[Flatten[Position[pAir, pOper]]];
```

Air Properties Calculation (Density and Viscosity)

```
 Dynamic Viscosity (μ) Calculation
σAir = 3.711; (* Characteristic molecular diameter in Armstrongs *)
eps = 78.6; (* K; ϵ/kB Characteristic Energy Parameter *)
tAdim = tAir / eps; (* Adimensional Temperature T*kB/ϵ *)
Ωn := Last[Last[Flatten[Solve[Log[y] ==
        -0.0129760904925 * Log[x] ^ 3 + 0.1165241107936 * Log[x] ^ 2 -
         0.4828286265717 * Log[x] + 0.4543932648609, y] /.
     x -> tAdim]]]
(* Collision Integral of the Enskog-Chapman Theory *)
μpoise := 2.67 * 10^-5 * Sqrt[mwAir * tAir] / (σAir^2 * Ωn); (* poise *)
μAir = μpoise / 10; (* kg/m-s *)
```

Calculation Dynamic Viscosity μ

Calculation of Terminal Velocity

As a function of Pressure and Temperature

```
ρAir = {};
velcharts = {};
reycharts = {};
estilos = {};
estilosT = {};
nombresP = {};
nombresT = {};
Do[ tOp[j] = tAir[[j]];
 μOp[j] = μAir[[j]];
 Clear[
  ρAirfunP, velchartsfunP, reychartsfunP, estilosfunP, nombresfunP];
ρAirfunP = {};
velchartsfunP = {};
reychartsfunP = {};
estilosfunP = {};
nombresfunP = {};
 Do[ρAi[i] := (Part[pAir, i] * 1.01 * 10^5) / (rAir * tOp[j]);
  (* kg/m^3; P in atm converted to Pa *)
ρAirfunP = Append[ρAirfunP, ρAi[i]];
velTerm[i] := ((partDiam * 10^-6) ^ 2) *
    gravAccel * (ρFe - ρAi[i]) / (18 * μOp[j]) * 100; (* cm/s *)
velchartsfunP = Append[velchartsfunP, velTerm[i]];
reynolds[i] := (partDiam * 10^-6) * (velTerm[i] / 100) * ρAi[i] / μOp[j];
reychartsfunP = Append[reychartsfunP, reynolds[i]];
estilo[i] := AbsoluteDashing[{i}];
estilosfunP = Append[estilosfunP, estilo[i]];
nombrefunP[i] := "P=" <> ToString[Part[pAir, i]];
nombresfunP =
   Append[nombresfunP, nombrefunP[i]];, {i, 1, Length[pAir]}];
 nombrefunT[j] := ToString[Part[tAir, j]] <> "K";
 nombresT = Append[nombresT, nombrefunT[j]];
 estilofunT[j] := AbsoluteDashing[{j}];
 estilosT = Append[estilosT, estilofunT[j]];
 ρAir = Append[ρAir, ρAirfunP];
 velcharts = Append[velcharts, velchartsfunP];
 reycharts = Append[reycharts, reychartsfunP];
 estilos = Append[estilos, estilosfunP];
 nombresP = Append[nombresP, nombresfunP];,
 {j, 1, Length[tAir]}];
```

Tabulation of Air Properties

```
precision = 4;
ρairtable = SetAccuracy[ρAir, precision];
μairtable = SetAccuracy[μAir * 1000, precision];
Print[
 "Density and Viscosity of Air vs. Pressure and Temperature"]
TableForm[Transpose[Insert[Transpose[ρairtable], μairtable, -1]],
 TableDirections -> {Column, Row}, TableHeadings ->
  {nombresT, Flatten[{First[nombresP], "   μ\n(centi\npoise)"}]},
 TableAlignments -> Center, ColumnSpacings -> 1]
```

Density and Viscosity of Air vs. Pressure and Temperature

	P=0.1	P=0.4	P=0.7	P=1.	μ (centi poise)
300K	0.117	0.469	0.821	1.173	0.018
600K	0.059	0.235	0.411	0.587	0.030
900K	0.039	0.156	0.274	0.391	0.039
1200K	0.029	0.117	0.205	0.293	0.047
1500K	0.023	0.094	0.164	0.235	0.054
1800K	0.020	0.078	0.137	0.196	0.061

Effect of Pressure on Terminal Velocity at Constant Temperature

```
(* Plot of Terminal
  Velocity vs. Pressure at different Temperatures *)
(* To obtain the individual plots, *)
(* remove the DisplayFunction -> Identity option *)
(* from the Plot instruction *)
allT = {};
Do[dummy = {};
 Do[
 plot[i] = Plot[Evaluate[Part[velcharts, i + 2 * (j - 1)]],
    {partDiam, 5, 75}, Frame -> True, AxesOrigin -> {0, 0},
    ImageSize -> 216, FrameLabel -> {"Particle Diameter (μm)",
      "Vel  cm/s ", StringJoin["Terminal Velocity at ",
       ToString[Part[tAir, i + 2 * (j - 1)]], " K"], None},
    Ticks -> Automatic, PlotStyle -> Part[estilos, i],
    PlotLegend -> Part[nombresP, i], LegendPosition -> {.65, -.4},
    LegendTextSpace -> 3, LegendShadow -> {0, 0},
    LegendLabel -> " Pressure", DisplayFunction -> Identity];
   dummy = Append[dummy, plot[i]];, {i, 1, 2}];
 allT = Append[allT, dummy];, {j, 1, Length[tAir] / 2}];
(* Plot
  of terminal velocity at tOper and pOper without any titles *)
Print["Terminal Velocity at "<>
  ToString[tOper]<>" K and "<>ToString[pOper]<>" Atm."]
Plot[Evaluate[velcharts[[posT, posP]]],
 {partDiam, 0, 50}, Frame -> True,
 ImageSize -> pagewidth, FrameLabel -> {"Particle Diameter (μm)",
   "Vel  cm/s ", (*StringJoin["Terminal Velocity at ",
     ToString[Part[tAir,4]]," K"]*)None, None},
 Ticks -> Automatic, AxesOrigin -> {0, 0}]
Show[GraphicsArray[allT, PlotRegion -> {{0, 1}, {0, 1}},
  GraphicsSpacing -> .05, ImageSize -> pagewidth]]
```

```
Terminal Velocity at 1800 K and 0.1 Atm.
```

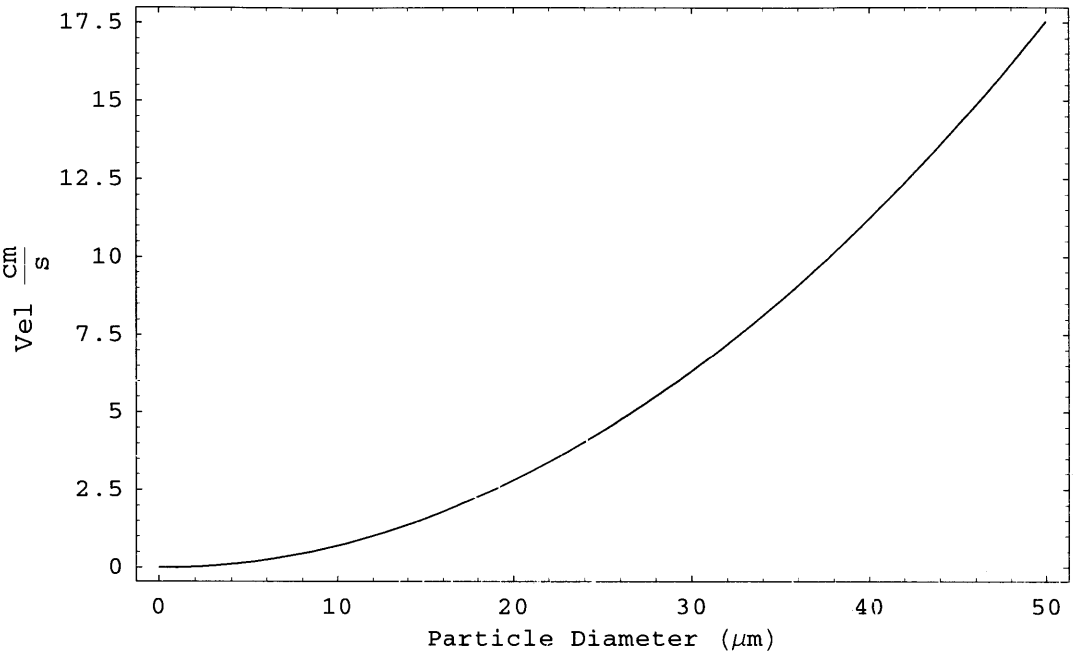
17.5
15
12.5
10
7.5
5
2.5
0
Vel cm/s
0
10
20
30
40
50
Particle Diameter (μm)

Graphics

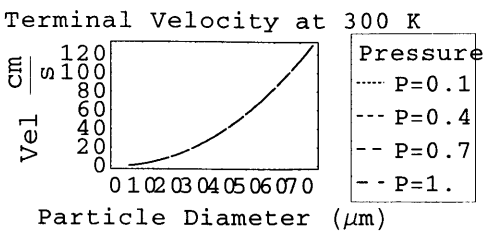

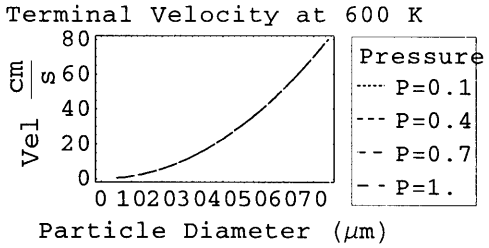

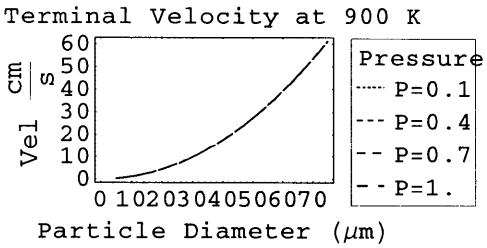

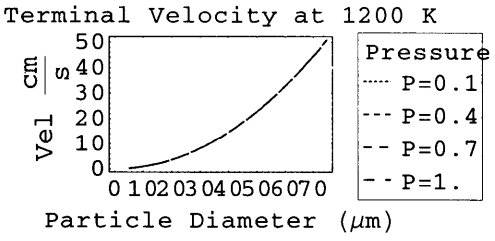

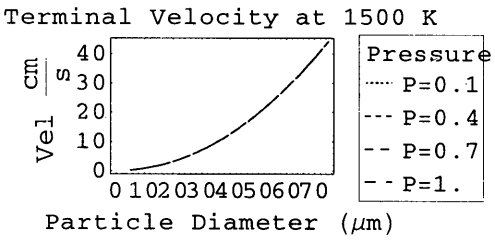

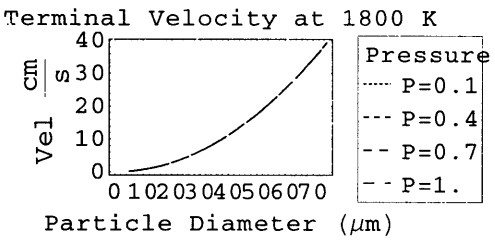

GraphicsArray

Effect of Temperature on Terminal Velocity at Constant Pressure

```
(* Plot of Terminal Velocity
   vs. Operating Temperature at 0.1 atm < P < 1 Atm *)
Plot[Evaluate[Flatten[Transpose[{First[Transpose[velcharts]]}]]],
 {partDiam, 0, 50},
 Frame -> True, ImageSize -> pagewidth, FrameLabel ->
  {"Particle Diameter (μm)", "Vel cm/s", "Terminal Velocity", None},
 Ticks -> Automatic, PlotStyle -> estilosT, PlotLegend -> nombresT,
  LegendPosition -> {.95, -.35}, LegendTextSpace -> 3,
 LegendShadow -> {0, 0}, LegendLabel -> "Temp (K)"]
```

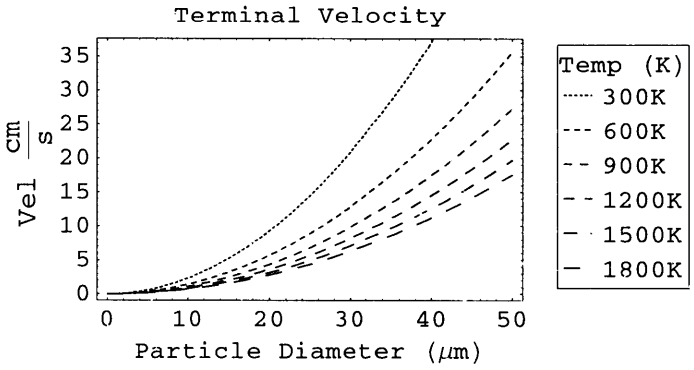

Graphics

Effect of Pressure on Particle Reynolds Number at Constant Temperature

```
reyT = {};
Do[dummy = {};
Do[plot[i] = Plot[Evaluate[Part[reycharts, i + 2 * (j - 1)]],
    {partDiam, 5, 50}, Frame -> True,
    ImageSize -> pagewidth, FrameLabel -> {"Particle Diameter (μm)",
      "Reynolds", StringJoin["Particle Reynolds\nNumber at ",
       ToString[Part[tAir, i + 2 * (j - 1)]], "K"], None},
    Ticks -> Automatic, PlotStyle -> Part[estilos, i],
    PlotLegend -> Part[nombresP, i], LegendPosition -> {.6, -.45},
    LegendShadow -> {0, 0}, LegendLabel -> " Pressure",
    LegendTextSpace -> 2.75, DisplayFunction -> Identity];
  dummy = Append[dummy, plot[i]];, {i, 1, 2}];
 reyT = Append[reyT, dummy];, {j, 1, Length[tAir] / 2}];
Show[GraphicsArray[reyT, PlotRegion -> {{0, 1}, {0, 1}},
  GraphicsSpacing -> .05, ImageSize -> pagewidth]]
```

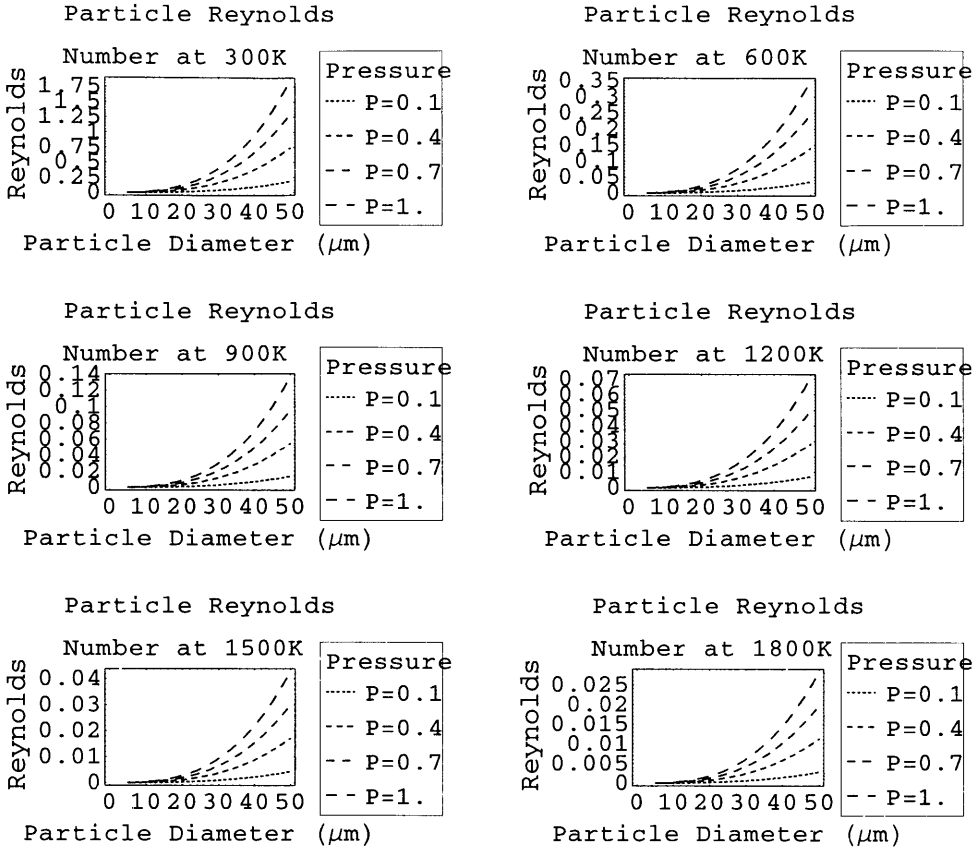

GraphicsArray

Effect of Temperature on Particle Reynolds Number at Constant Pressure

```
(* Plot of Reynold vs. Part. Diameter *)
(* To obtain the individual plots,
 remove the DisplayFunction -> *)
 (* Identity option from the Plot instruction *)
reyP = {};
reycharts2 = Transpose[reycharts];
Do[dummy = {};
 Do[plot[i] = Plot[Evaluate[Part[reycharts2, i + 2 * (j - 1)]],
    {partDiam, 5, 50}, Frame -> True, ImageSize -> pagewidth,
    FrameLabel -> {"Particle Diameter (μm)",
      "Reynolds", StringJoin["Particle Reynolds\nNumber at ",
       ToString[Part[pAir, i + 2 * (j - 1)]], " Atm"], None},
    Ticks -> Automatic, PlotStyle -> Part[estilosT, i],
    PlotLegend -> nombresT, LegendPosition -> {.65, -.4},
    LegendShadow -> {0, 0}, LegendLabel -> "Temp",
    LegendTextSpace -> 3.5, DisplayFunction -> Identity];
   dummy = Append[dummy, plot[i]];, {i, 1, 2}];
 reyP = Append[reyP, dummy];, {j, 1, Length[pAir] / 2}];
Show[GraphicsArray[reyP, PlotRegion -> {{0, 1}, {0, 1}},
  GraphicsSpacing -> .05, ImageSize -> pagewidth]]
```

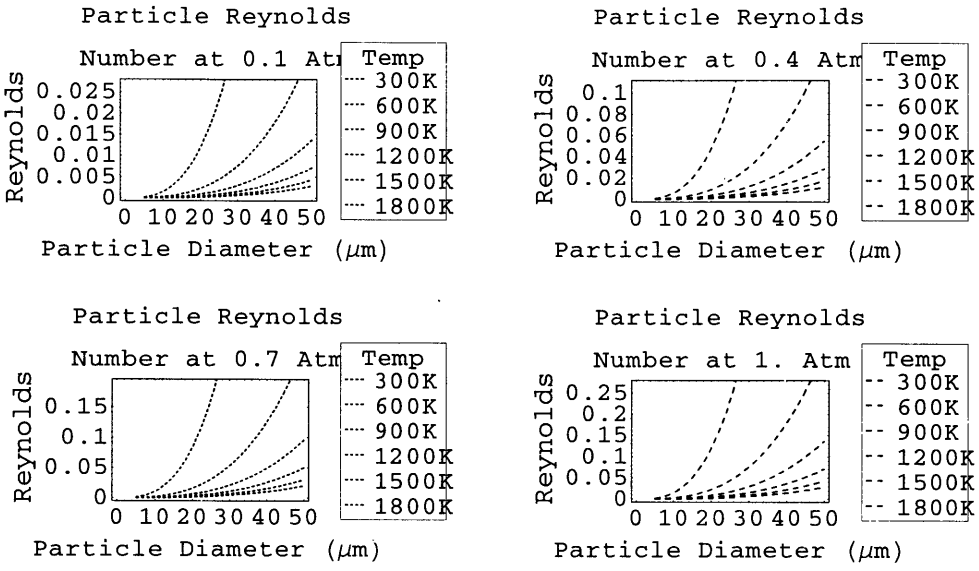

GraphicsArray

Residence Time vs. Flight Distance Assuming Constant Particle Velocity

```
dipar = Range[10, 50, 10]; (* μm *)
estilaisho =
 Map[AbsoluteDashing, Partition[dipar / Length[dipar], 1]];
restimedist =
 lengthfd / velcharts[[posT, posP]] /. partDiam -> dipar ;
(* length in cm *)
Plot[Evaluate[restimedist], {lengthfd, 0, 100}, Frame -> True,
 AxesOrigin -> Automatic, FrameLabel -> {"Fligth Distance (cm)",
   "Time (s)", (*StringJoin["Residence Time at ",
     ToString[Part[tAir,4]],                " K "]*)" ", None},
 Ticks -> Automatic, PlotStyle -> estilaisho, PlotLegend -> dipar,
 LegendPosition -> {.95, -.35}, LegendShadow -> {0, 0},
 LegendLabel -> "Dp (μm)", LegendTextSpace -> 2.5,
 ImageSize -> pagewidth]
```

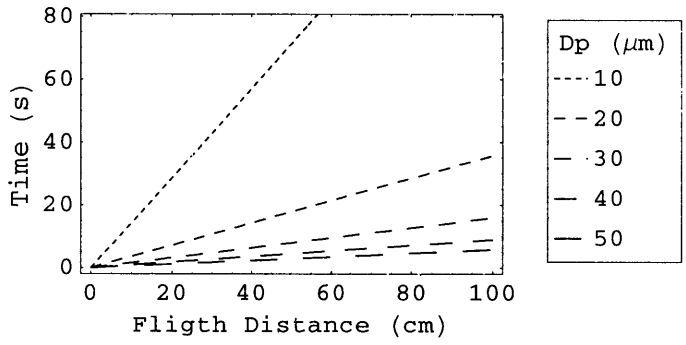

Graphics

Residence Time vs. Particle Diameter Assuming Particle Falls at Terminal Velocity (Validated in next Subsection)

```
resTime = furHotLength * 100 / velcharts[[posT, posP]]; (* s *)
dpmin = 5;
dpmax = 50;
dpminzoom1 = 10;
dpmaxzoom1 = 50;
dpminzoom2 = 50;
dpmaxzoom2 = 125;
Plot[resTime, {partDiam, dpmin, dpmax}, Frame -> True,
 AxesOrigin -> {0, 0}, FrameLabel -> {"Particle Diameter (μm)",
   "Time (s)", StringJoin["Residence Time at ",
    ToString[tOper], " K and ", ToString[pOper], " Atm"], None},
 ImageSize -> pagewidth]
Plot[resTime, {partDiam, dpminzoom1, dpmaxzoom1},
 Frame -> True, AxesOrigin -> {dpminzoom1, 0},
 FrameLabel -> {"Particle Diameter (μm)", "Time (s)",
   StringJoin["Residence Time at ", ToString[tOper],
    " K and ", ToString[pOper], " Atm"](*" "*), None},
 ImageSize -> pagewidth]
Plot[resTime, {partDiam, dpminzoom2, dpmaxzoom2},
 Frame -> True, AxesOrigin -> {dpminzoom2, 0},
 FrameLabel -> {"Particle Diameter (μm)",
   "Time (s)", StringJoin["Residence Time at ",
    ToString[tOper], " K and ", ToString[pOper], " Atm"], None},
 ImageSize -> pagewidth]
```

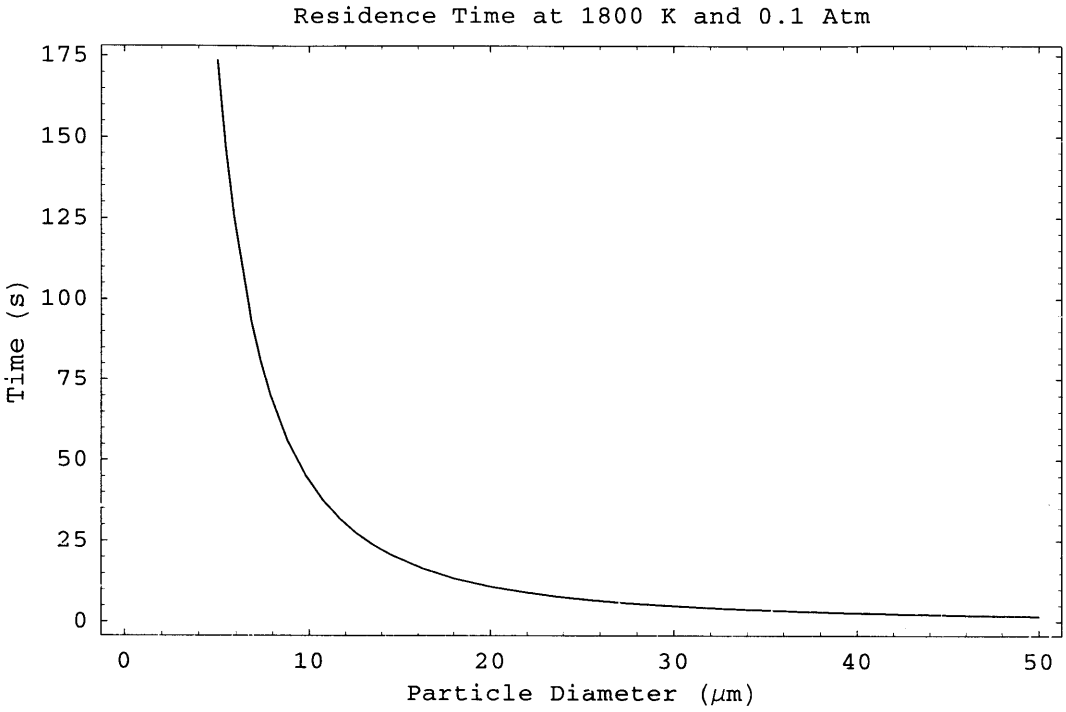
Residence Time at 1800 K and 0.1 Atm
Time (s)
175
150
125
100
75
50
25
0
0
10
20
30
40
50
Particle Diameter (μm)

Graphics

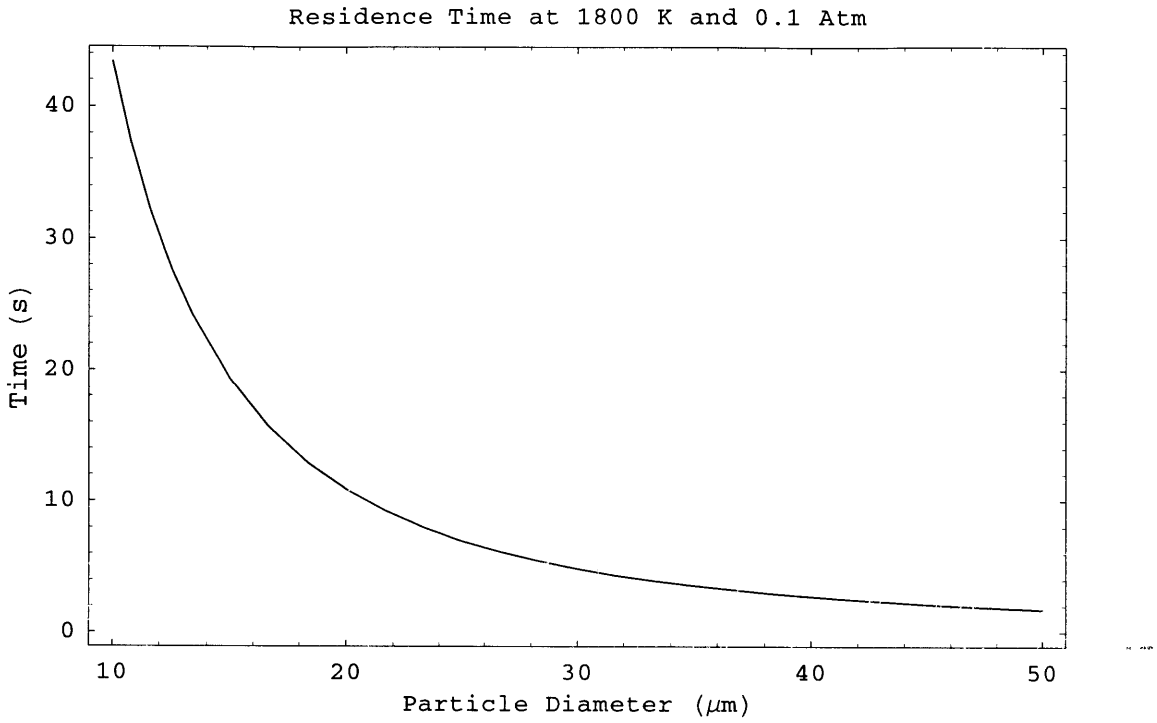
Residence Time at 1800 K and 0.1 Atm
Time (s)
0
10
20
30
40
10
20
30
40
50
Particle Diameter (μm)

Graphics

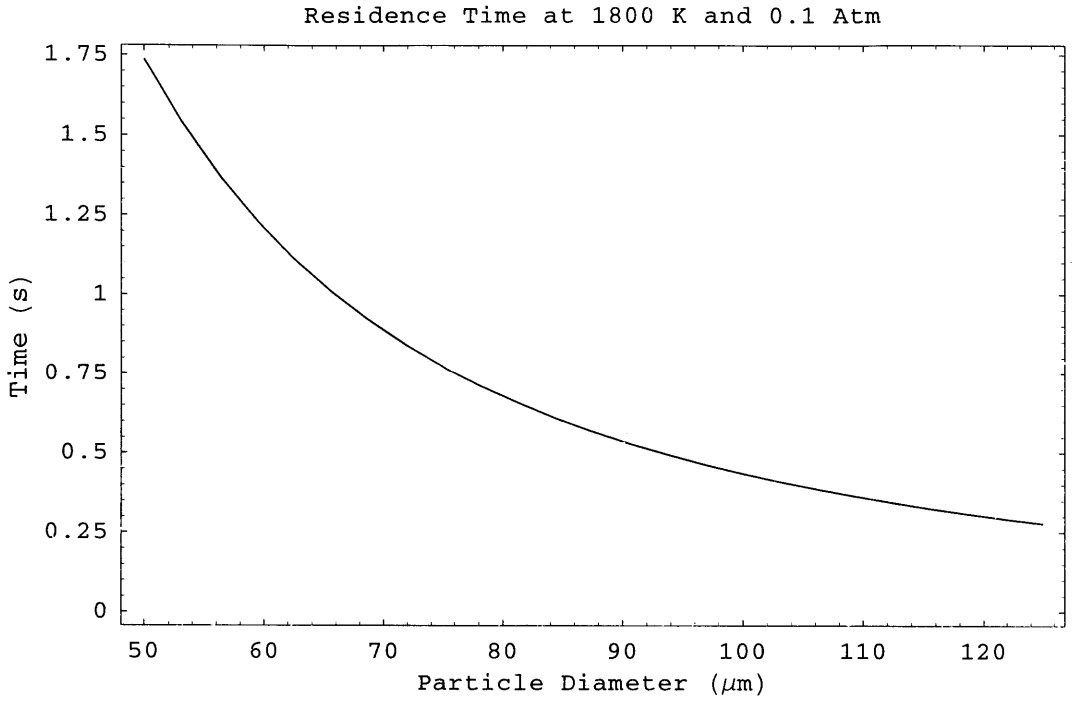
Residence Time at 1800 K and 0.1 Atm
Time (s)
1.75
1.5
1.25
1
0.75
0.5
0.25
0
50
60
70
80
90
100
110
120
Particle Diameter (μm)

Graphics

Time to Reach Terminal Velocity

```
μOper = μAir[[posT]];
ρOper = ρAir[[posT, posP]];
Do[
estilacho = {};
plot1 = {};
dp = Range[2 * 5^j, 5^(j+1), 5^j] * 10^-6;
nombress = Flatten[Map[List, dp * 10^6]];
 Do[
estilach[i] = Dashing[{i / 100}];
estilacho = Append[estilacho, estilach[i]];
Clear[vp, a, n, t, len, lenvelplot];
a[0] = 0;
vp[0] = 0;
t[0] = 0;
len[0] = 0;
n = 11000 - j^6 * 1000^j * dp[[i]];
len[t_] := len[t] = len[t - 1] + vp[t] / n + 0.5 * a[t] * (1 / n)^2;
vp[t_] := vp[t] = vp[t - 1] + a[t - 1] / n;
a[t_] := a[t] = 1/(dp[[i]]^3 * ρFe) (-18 * dp[[i]] * vp[t] * μOper +
        dp[[i]]^3 * gravAccel * (ρFe - ρOper));
lenvelplot = Table[{len[k], vp[k]}, {k, 0, 100 * j^3}] * 100;
plot1 = Append[plot1, lenvelplot];, {i, 1, Length[dp]}];
Apply[MultipleListPlot,
  Append[plot1, {PlotJoined -> True, Frame -> True, FrameLabel ->
     {"Length (cm)", "Vel cm/s", StringJoin["Initial Velocity at ",
       ToString[tOper], " K and ", ToString[pOper], "Atm"], None},
    Ticks -> Automatic, SymbolStyle -> None,
    SymbolShape -> None, PlotStyle -> estilacho,
    PlotLegend -> nombress, LegendPosition -> {1, -.35},
    LegendTextSpace -> 1.5, LegendShadow -> {0, 0},
    LegendLabel -> "Dp (μm)", ImageSize -> pagewidth}]],
 {j, 1, 2}];
```

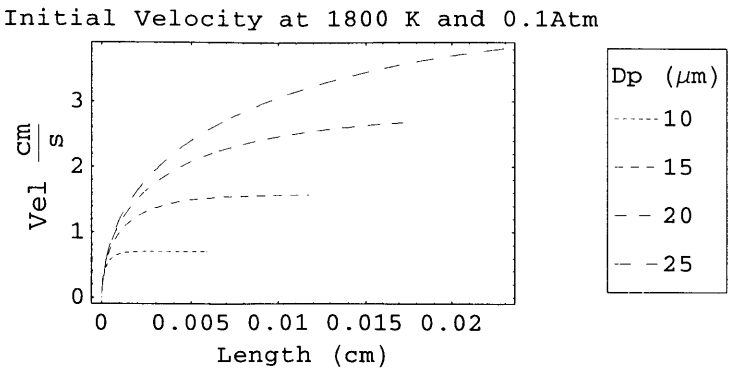

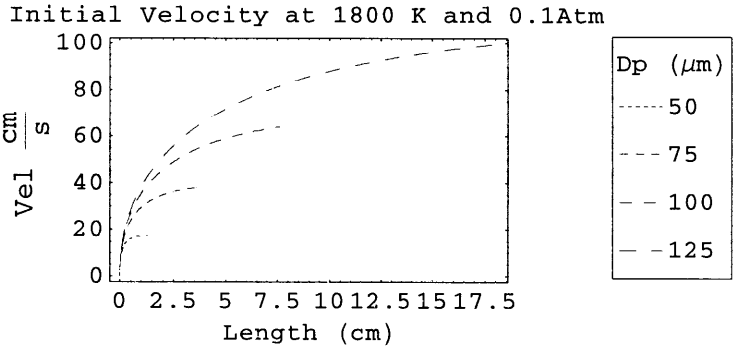

Check on Natural Convection

Operating Parameters

```
kAir = 6.375933728 * 10^-12 * tAir^3 - 32562.86150437 * 10^-12 * tAir^2 +
  92676008.44008020 * 10^-12 * tAir + 1290679682.61412000 * 10^-12;
cpAir = 944.08 + 0.1908 * tAir;
```

Calculation of Adimensional Numbers

```
(* Calculation of Prandtl, Grashof and Rayleigh *)
prandtl = cpAir * μAir / kAir;
tW = tAir + 50;
pTube = pOper * 1.01 * 10^5; (* Pa *)
ρOper = ρAir[[posT, posP]];
gras = gravAccel * furHotLength^3 * (ρOper^2 / μAir^2) * (tW - tAir) / tAir;
rayleigh = prandtl * gras;
(* Tabulation of Adimensional Numbers (at Operating Pressure) *)
Print["Adimensional Numbers at "<>ToString[pOper]<>" Atm"]
TableForm[{tAir, kAir, prandtl, gras, rayleigh},
 TableDirections -> {Row, Column}, TableHeadings -> {{"Temp\n(K)",
    "k-Air\n J/(m-s-K)", "Prandtl", "Grashof", "Rayleigh"}, None},
 TableAlignments -> Center]
```

Adimensional Numbers at 0.1 Atm

Temp (K)	k-Air $\frac{J}{m-s-K}$	Prandtl	Grashof	Rayleigh
300	0.026335	0.697234	52628.4	36694.3
600	0.0465509	0.678402	9941.86	6744.58
900	0.0629712	0.689961	3890.58	2684.35
1200	0.076629	0.716758	2018.04	1446.45
1500	0.088557	0.749525	1215.95	911.386
1800	0.0997883	0.781445	804.076	628.341

■ *Particle Heat Transfer Model*

Materials Thermal Properties

```
εFe = 0.65;
CpFe = 460; (* J/kg-K *)
hFe = 126000; (* J/kg  Latent Heat of Fusion *)
DeltaT = 5;
CpEff = CpFe + hFe / DeltaT;
CpLiq = 824; (* J/Kg-K *)
σ = 5.6705 * 10^-8; (* W/m^2-K^4 *)
tWalls = 1575 + 273; (* K *)
tMelt = 1535 + 273; (* K *)
tInitial = 25 + 273; (* K *)
kFeInitial = 80.3; (* W/m-k; at 300 K *)
chop[{}] = {}
chop[{{}, {}}] = {};
chop[{x__, {}}] = {x};
chop[{x__, y___}] :=
 Join[{x}, If[Last[x] == Last[First[{y}]], {}, chop[{y}]]];
chopi[{{}, {}}] = {};
chopi[{x__, {}}] = {x};
chopi[{x__, y___}] :=
 Join[{x}, If[TrueQ[Head[First[{y}]] == Complex], {}, chopi[{y}]]];
```

```
{}
```

Check for Lumped Parameter Approach Validation

```
hConv = 0;
hRad = ϵFe * σ * (tInitial^4 - tWalls^4) / (tInitial - tWalls);
hTot = hConv + hRad;
biot = (hTot / kFeInitial) * (partDiam * 10^-6) /.
  partDiam -> Range[10, 100, 10];
NumberForm[TableForm[{Range[10, 100, 10], biot},
  TableDirections -> {Row, Column}, TableHeadings ->
   {{"Dp", "Biot"}, None}, TableAlignments -> Center],
 precision]
```

Dp	Biot
10	0.00003451
20	0.00006903
30	0.0001035
40	0.0001381
50	0.0001726
60	0.0002071
70	0.0002416
80	0.0002761
90	0.0003106
100	0.0003451

Particle Heating -- Time To reach Melting Point (Assuming particle falls at terminal velocity)

```
timeToMeltPnt =
 Solve[Integrate[1 / (tWalls^4 - temp^4), {temp, tInitial, tMelt}] ==
   Integrate[ 6 * σ * ϵFe / (ρFe * CpFe * Dp * 10^-6) , {q, 0, t}], t];
timetomeltpoint = Last[Last[Flatten[timeToMeltPnt]]];
Plot[timetomeltpoint, {Dp, 5, 100}, Frame -> True,
 FrameLabel -> {"Particle Diameter (μm)", "Time (s)",
   "Time to Reach Melting Point", None}]
```

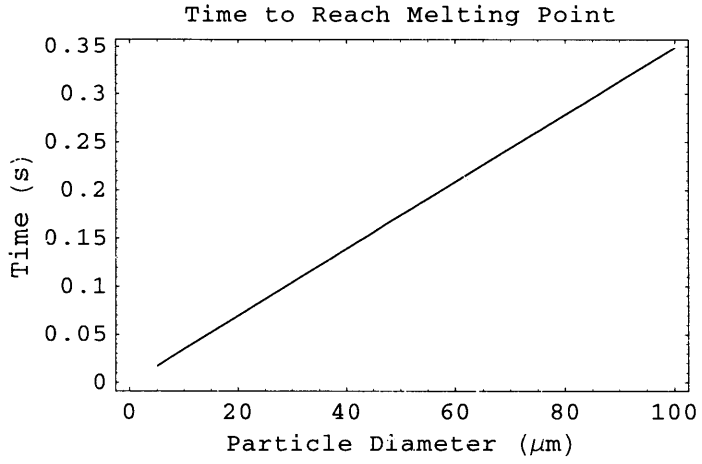

Graphics

Particle Melting - Time To Melt

```
timeToMelt = Solve[
  Integrate[1 / (tWalls^4 - temp^4), {temp, tMelt, tMelt + DeltaT}] ==
   Integrate[ 6 * σ * ϵFe / (ρFe * CpEff * Dp * 10^-6), {q, 0, t}], t];
timetomelt = Last[Last[Flatten[timeToMelt]]];
totaltime = timetomeltpoint + timetomelt;
velpart = velcharts[[posT, posP]];
len = totaltime * velpart /. Dp -> partDiam;
dmax = Last[Last[Last[Solve[dist == len, partDiam]]]];
Plot[dmax, {dist, 0, 30}, Frame -> True,
 FrameLabel -> {"Flight Distance (cm)", "Dp (μ)",
   "Required Distance to Melt\nat "<>ToString[tOper]<>
    " K and "<>ToString[pOper]<>" Atm."(*" "*), None},
 ImageSize -> pagewidth]
(*  Plot[timetomelt,{Dp,5,100},Frame->True, FrameLabel->
   {"Particle Diameter (μm)","Time (s)","Time to Melt",None}]*)
(* Plot[totaltime,{Dp,5,100},
  Frame->True, FrameLabel->{"Particle Diameter (μm)",
    "Time (s)","Total Time to Melt",None},
  ImageSize->pagewidth] *)
```

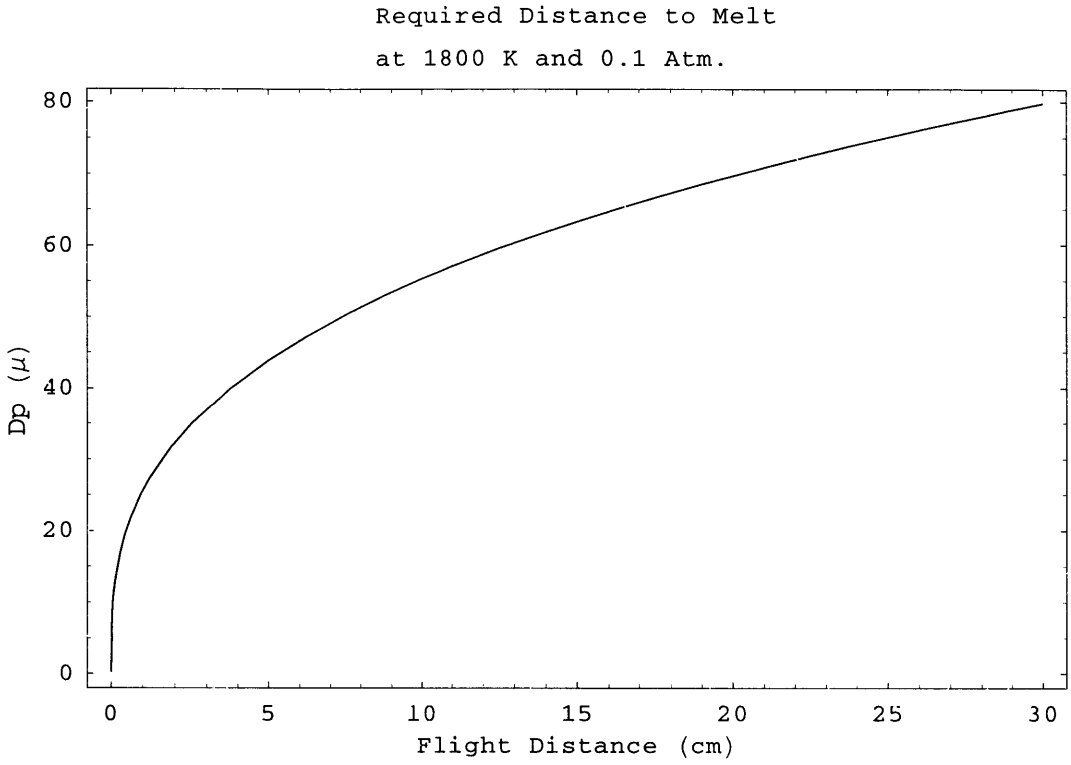
Required Distance to Melt
at 1800 K and 0.1 Atm.
80
60
40
20
0
Dp (μ)
0
5
10
15
20
25
30
Flight Distance (cm)

Graphics

Particle Temperature Calculation

Particle Heating in Pre-Heating Zone of Furnace

```
Clear[x, length, temper, temp1, tWalls1, deltatime]
dp = 50; (* particle Diameter in microns *)
lengthzone1 = 13 * 2.54; (* cm *)
tini1 = 300; (* K *)
totaltimezone1 =
 lengthzone1 / velcharts[[posT, posP]] /. partDiam -> dp;
(* seconds *)
deltatime = 1 / 100 ; (* step of time increments in seconds *)
length = deltatime * velcharts[[posT, posP]] /. partDiam -> dp;
(* length step in centimeters *)
tWalls1[x_] := tWalls1[x] =
  If[x * length < 4 * 2.54, 560, 942.44 Log[x * length] - 1577.6];
(* Approximation
  to experimental values of tube wall temperature *)
temper[x_] := temper[x] =
  temp1 /. FindRoot[ 1/(4 * tWalls1[x]^3) (2 * ArcTan[temp1/tWalls1[x]] -
        Log[-temp1 + tWalls1[x]] + Log[temp1 + tWalls1[x]]) -
      1/(4 * tWalls1[x]^3) (2 * ArcTan[tini1/tWalls1[x]] -
        Log[-tini1 + tWalls1[x]] + Log[tini1 + tWalls1[x]]) ==
    (6 * σ * εFe * x * deltatime) / (ρFe * CpFe * dp * 10^-6),
   {temp1, tWalls1[x] - 50}, WorkingPrecision -> 17];
zone1 = Table[{N[k * length, 4], N[temper[k], 6]},
  {k, 0, totaltimezone1 / deltatime, 10}];
allzone1 = Table[{N[k * deltatime, 4],
   N[k * length, 4], N[tWalls1[k], 6], N[temper[k], 6]},
  {k, 0, totaltimezone1 / deltatime, 10}];
TableForm[allzone1, TableDirections -> {Column, Row},
 TableHeadings -> {None, {"Time\n (s)\n",
    "Position\n  (cm)\n", "TWall\n (K)\n", "Tpart\n (K)\n"}},
 TableAlignments -> Center];
```

Particle Heating in Hot Zone of Furnace up to Melting Point

```
Clear[x, length, temper, temp2, tWalls2, deltatime];
tmmin = 1535 + 273;
tmmax = 1540 + 273;
(* dp=50; particle Diameter in microns *)
lengthzone2 = 11 * 2.54; (* cm *)
tini2 = Last[Last[zone1]]; (* K *)
totaltimezone2 =
 lengthzone2 / velcharts[[posT, posP]] /. partDiam -> dp;
(* seconds *)
deltatime = 1 / 100 ; (* step of time increments in seconds *)
length = deltatime * velcharts[[posT, posP]] /. partDiam -> dp;
(* length step in centimeters *)
tWalls2[x_] :=
 tWalls2[x] = -0.0014 * (x * length)^4 + 0.0782 * (x * length)^3 -
   1.9171 * (x * length)^2 + 23.026 * (x * length) + 1752.9 ;
(* Approximation
  to experimental values of tube wall temperature *)
temper[0] = tini2;
temper[x_] := temper[x] = If[temper[x - 1] ≥ tmmin, tmmin,
  temp2 /. FindRoot[ 1/(4 * tWalls2[x]^3) (2 * ArcTan[temp2/tWalls2[x]] -
          Log[-temp2 + tWalls2[x]] + Log[temp2 + tWalls2[x]]) -
        1/(4 * tWalls2[x]^3) (2 * ArcTan[tini2/tWalls2[x]] -
          Log[-tini2 + tWalls2[x]] + Log[tini2 + tWalls2[x]]) ==
      (6 * σ * εFe * x * deltatime) / (ρFe * CpFe * dp * 10^-6),
    {temp2, tWalls2[x] - 5.0}, WorkingPrecision -> 17]];
 zone2pre = Table[{N[k * length, 4], N[temper[k], 6]},
  {k, 0, totaltimezone2 / (2 * deltatime), 1}];
If[zone2pre[[Length[zone2pre] - 1, 2]] == Last[Last[zone2pre]],
 zone2 = chop[zone2pre], zone2 = zone2pre];
allzone2 = Table[{N[k * deltatime + First[Last[allzone1]], 4],
   N[k * length + allzone1[[Length[allzone1], 2]], 4],
   N[tWalls2[k], 6], N[temper[k], 6]}, {k, 0, First[Last[zone2]] /
    (deltatime * velcharts[[posT, posP]] /. partDiam -> dp), 1}];
TableForm[allzone2, TableDirections -> {Column, Row},
 TableHeadings -> {None, {"Time\n (s)\n",
```

```
    "Position\n  (cm)\n", "TWall\n (K)", "Tpart\n (K)"}},
 TableAlignments -> Center];
```

Particle Melting in Hot Zone

```
Clear[x, length, temper, temp3, tWalls3, deltatime];
tmmin = 1535 + 273;
tmmax = 1540 + 273;
(* dp=50; particle Diameter in microns *)
lengthzone3 = 11 * 2.54 - First[Last[zone2]]; (* cm *)
tini3 = Last[Last[zone2]]; (* K *)
totaltimezone3 =
 lengthzone3 / velcharts[[posT, posP]] /. partDiam -> dp;
(* seconds *)
deltatime = 1 / 100 ; (* step of time increments in seconds *)
length = deltatime * velcharts[[posT, posP]] /. partDiam -> dp;
(* length step in centimeters *)
llen = First[Last[zone2]];
(* Length at which zone2 changes to zone3 *)
tWalls3[x_] := tWalls3[x] =
  -0.0014 * (x * length + llen) ^ 4 + 0.0782 * (x * length + llen)^3 -
   1.9171 * (x * length + llen) ^ 2 + 23.026 * (x * length + llen) + 1752.9 ;
(* Approximation
  to experimental values of tube wall temperature *)
temper[0] = tini3;
temper[x_] := temper[x] = If[temper[x - 1] ≥ tmmax, tmmax,
  temp3 /. FindRoot[ 1/(4 * tWalls3[x]^3) (2 * ArcTan[ temp3/tWalls3[x] ] -
          Log[-temp3 + tWalls3[x]] + Log[temp3 + tWalls3[x]]) -
        1/(4 * tWalls3[x]^3) (2 * ArcTan[ tmmin/tWalls3[x] ] -
          Log[-tmmin + tWalls3[x]] + Log[tmmin + tWalls3[x]]) ==
      (6 * σ * εFe * x * deltatime) / (ρFe * CpEff * dp * 10^-6),
    {temp3, temper[x - 1] + 1.0}, WorkingPrecision -> 17]];
zone3pre = Table[{N[k * length + llen, 4], N[temper[k], 6]},
  {k, 0, totaltimezone3 / (deltatime), 1}];
If[zone3pre[[Length[zone3pre] - 1, 2]] == Last[Last[zone3pre]],
 zone3 = chop[zone3pre], zone3 = zone3pre];
```

```
allzone3 = Table[{N[k * deltatime + First[Last[allzone2]], 4],
   N[k * length + allzone2[[Length[allzone2], 2]], 4],
   N[tWalls3[k], 6], N[temper[k], 6]},
  {k, 0, (First[Last[zone3]] - llen) /
    (deltatime * velcharts[[posT, posP]] /. partDiam -> dp), 1}];
TableForm[allzone3, TableDirections -> {Column, Row},
 TableHeadings -> {None, {"Time\n (s)\n",
    "Position\n  (cm)\n", "TWall\n (K)", "Tpart\n (K)"}},
 TableAlignments -> Center];
```

Superheating in Hot Zone

```
Clear[x, length, temper, temp4, tWalls4, deltatime, llen];
tmmin = 1535 + 273;
tmmax = 1540 + 273;
lengthzone4 = 11 * 2.54 - First[Last[zone3]]; (* cm *)
tini4 = Last[Last[zone3]]; (* K *)
totaltimezone4 =
 lengthzone4 / velcharts[[posT, posP]] /. partDiam -> dp;
(* seconds *)
deltatime = 1 / 100 ; (* step of time increments in seconds *)
length = deltatime * velcharts[[posT, posP]] /. partDiam -> dp;
(* length step in centimeters *)
llen = First[Last[zone3]];
(* Length at which zone3 changes to zone4 *)
tWalls4[x_] := tWalls4[x] =
  -0.0014 * (x * length + llen) ^ 4 + 0.0782 * (x * length + llen)^3 -
   1.9171 * (x * length + llen) ^ 2 + 23.026 * (x * length + llen) + 1752.9 ;
(* Approximation
  to experimental values of tube wall temperature *)
temper[0] = tini4;
temper[x_] := temper[x] =
  If[ (*temper[x]<tmmax*)TrueQ[Head[temper[x - 1] == Complex]],
   tmmax, temp4 /. FindRoot[ 1/(4 * tWalls4[x]^3) (2 * ArcTan[ temp4/tWalls4[x] ] -
          Log[-temp4 + tWalls4[x]] + Log[temp4 + tWalls4[x]]) -
        1/(4 * tWalls4[x]^3) (2 * ArcTan[ tmmax/tWalls4[x] ] -
          Log[-tmmax + tWalls4[x]] + Log[tmmax + tWalls4[x]]) ==
       (6 * σ * εFe * x * deltatime) / (ρFe * CpLiq * dp * 10^-6),
```

```
      {temp4, tWalls4[x] - .5}, WorkingPrecision -> 17]];
zone4pre =
 Table[N[temper[k], 6], {k, 0, totaltimezone4 / (deltatime), 1}];
zone4pre2 = chopi[zone4pre];
zone4 = Table[
  {N[k * length + llen, 4], zone4pre2[[k]]}, {k, 1, Length[zone4pre2]}];
allzone4 = Table[{N[k * deltatime + First[Last[allzone3]], 4],
   N[k * length + allzone3[[Length[allzone3], 2]], 4],
   N[tWalls4[k], 6], N[temper[k], 6]}, {k, 0, Length[zone4pre2] - 1}];
TableForm[allzone4, TableDirections -> {Column, Row},
 TableHeadings -> {None, {"Time\n (s)\n",
    "Position\n  (cm)\n", "TWall\n (K)", "Tpart\n (K)"}},
 TableAlignments -> Center];
```

Particle Solidification in Hot Zone

```
Clear[x, length, temper, temp5, tWalls5, deltatime, llen];
tmmin = 1535 + 273;
tmmax = 1540 + 273;
lengthzone5 = 11 * 2.54 - First[Last[zone4]]; (* cm *)
tini5 = Last[Last[zone4]]; (* K *)
totaltimezone5 =
 lengthzone5 / velcharts[[posT, posP]] /. partDiam -> dp;
(* seconds *)
deltatime = 1 / 100 ; (* step of time increments in seconds *)
length = deltatime * velcharts[[posT, posP]] /. partDiam -> dp;
(* length step in centimeters *)
llen = First[Last[zone4]];
(* Length at which zone4 changes to zone5 *)
tWalls5[x_] := tWalls5[x] =
  -0.0014 * (x * length + llen) ^ 4 + 0.0782 * (x * length + llen)^3 -
   1.9171 * (x * length + llen) ^ 2 + 23.026 * (x * length + llen) + 1752.9 ;
(* Approximation
  to experimental values of tube wall temperature *)
temper[0] = tini5;
temper[x_] := temper[x] = If[temper[x - 1] ≤ tmmin, tmmin,
  temp5 /. FindRoot[ 1/(4 * tWalls5[x]^3) (2 * ArcTan[ temp5/tWalls5[x] ] -
          Log[-temp5 + tWalls5[x]] + Log[temp5 + tWalls5[x]]) -
       1/(4 * tWalls5[x]^3) (2 * ArcTan[ tmmax/tWalls5[x] ] -
```

```
          Log[-tmmax + tWalls5[x]] + Log[tmmax + tWalls5[x]]) ==
       (6 * σ * ϵFe * x * deltatime) / (ρFe * CpEff * dp * 10^-6),
      {temp5, temper[x - 1] - .5}, WorkingPrecision -> 17]];
zone5pre = Table[{N[k * length + llen, 4], N[temper[k], 6]},
  {k, 0, totaltimezone5 / (deltatime), 1}];
If[zone5pre[[Length[zone5pre] - 1, 2]] == Last[Last[zone5pre]],
 zone5 = chop[zone5pre], zone5 = zone5pre];
allzone5 = Table[{N[k * deltatime + First[Last[allzone4]], 4],
   N[k * length + allzone4[[Length[allzone4], 2]], 4],
   N[tWalls5[k], 6], N[temper[k], 6]},
  {k, 0, (First[Last[zone5]] - llen) /
    (deltatime * velcharts[[posT, posP]] /. partDiam -> dp), 1}];
TableForm[allzone5, TableDirections -> {Column, Row},
 TableHeadings -> {None, {"Time\n (s)\n",
    "Position\n  (cm)\n", "TWall\n (K)", "Tpart\n (K)"}},
 TableAlignments -> Center];
```

Particle Solidification in Cooling Zone
(If Solidification Does Not End in Hot Zone)

```
Clear[x, length, temper, temp6, tWalls6, deltatime, llen];
tmmin = 1535 + 273;
tmmax = 1540 + 273;
lengthzone6 = 10 * 2.54; (* cm *)
tini6 = Last[Last[zone5]]; (* K *)
totaltimezone6 =
 lengthzone6 / velcharts[[posT, posP]] /. partDiam -> dp;
(* seconds *)
deltatime = 1 / 100 ; (* step of time increments in seconds *)
length = deltatime * velcharts[[posT, posP]] /. partDiam -> dp;
(* length step in centimeters *)
llen = 0.0;
(* Length at which zone5 changes to zone6 *)
tWalls6[x_] := tWalls6[x] = 0.0936 * (x * length + llen)^3 -
   2.9228 * (x * length + llen) ^ 2 - 33.539 * (x * length + llen) + 1762;
(* Approximation
  to experimental values of tube wall temperature *)
temper[0] = tini6;
temper[x_] := temper[x] = If[temper[x - 1] ≤ tmmin, tmmin,
  temp6 /. FindRoot[ 1/(4 * tWalls6[x]^3) (2 * ArcTan[ temp6/tWalls6[x] ] -
```

```
        Log[-temp6 + tWalls6[x]] + Log[temp6 + tWalls6[x]]) -
      1
  4 * tWalls6[x]^3 (2 * ArcTan[ tini6 / tWalls6[x] ] -
        Log[-tini6 + tWalls6[x]] + Log[tini6 + tWalls6[x]]) ==
    (6 * σ * ϵFe * x * deltatime) / (ρFe * CpEff * dp * 10^-6),
   {temp6, temper[x - 1] - .5}, WorkingPrecision -> 17]];
zone6pre = Table[{N[k * length + llen, 4], N[temper[k], 6]},
  {k, 0, totaltimezone6 / (deltatime), 1}];
If[zone6pre[[Length[zone6pre] - 1, 2]] == Last[Last[zone6pre]],
 zone6 = chop[zone6pre], zone6 = zone6pre];
allzone6 = Table[{N[k * deltatime + First[Last[allzone5]], 4],
   N[k * length + allzone5[[Length[allzone5], 2]], 4],
   N[tWalls6[k], 6], N[temper[k], 6]},
  {k, 0, (First[Last[zone6]] - llen) /
    (deltatime * velcharts[[posT, posP]] /. partDiam -> dp), 1}];
TableForm[allzone6, TableDirections -> {Column, Row},
 TableHeadings -> {None, {"Time\n (s)\n",
    "Position\n  (cm)\n", "TWall\n (K)", "Tpart\n (K)"}},
 TableAlignments -> Center];
```

Particle Cooling in Cooling Zone of Furnace

```
Clear[x, length, temper, temp7, tWalls7, deltatime, llen];
tmmin = 1535 + 273;
tmmax = 1540 + 273;
lengthzone7 = 10 * 2.54 - First[Last[zone6]]; (* cm *)
tini7 = Last[Last[zone6]]; (* K *)
totaltimezone7 =
 lengthzone7 / velcharts[[posT, posP]] /. partDiam -> dp;
(* seconds *)
deltatime = 1 / 100 ; (* step of time increments in seconds *)
length = deltatime * velcharts[[posT, posP]] /. partDiam -> dp;
(* length step in centimeters *)
llen = First[Last[zone6]];
(* Length at which zone6 changes to zone7 *)
tWalls7[x_] := tWalls7[x] = 0.0936 * (x * length + llen)^3 -
   2.9228 * (x * length + llen)^2 - 33.539 * (x * length + llen) + 1762;
(* Approximation
  to experimental values of tube wall temperature *)
temper[0] = tini7;
```

```
temper[x_] := temper[x] = If[temper[x - 1] > tmmin, tmmin,
  temp7 /. FindRoot[ 1/(4 * tWalls7[x]^3) (2 * ArcTan[ temp7/tWalls7[x] ] -
          Log[-temp7 + tWalls7[x]] + Log[temp7 + tWalls7[x]]) -
        1/(4 * tWalls7[x]^3) (2 * ArcTan[ tmmin/tWalls7[x] ] -
          Log[-tmmin + tWalls7[x]] + Log[tmmin + tWalls7[x]]) ==
       (6 * σ * εFe * x * deltatime) / (ρFe * CpFe * dp * 10^-6),
     {temp7, temper[x - 1] - .5}, WorkingPrecision -> 17]];
zone7pre = Table[{N[k * length + llen, 4], N[temper[k], 6]},
  {k, 0, totaltimezone7 / (deltatime), 1}];
If[zone7pre[[Length[zone7pre] - 1, 2]] == Last[Last[zone7pre]],
 zone7 = chop[zone7pre], zone7 = zone7pre];
allzone7 = Table[{N[k * deltatime + First[Last[allzone6]], 4],
   N[k * length + allzone6[[Length[allzone6], 2]], 4],
   N[tWalls7[k], 6], N[temper[k], 6]},
  {k, 0, (First[Last[zone7]] - llen) /
    (deltatime * velcharts[[posT, posP]] /. partDiam -> dp), 1}];
TableForm[allzone7, TableDirections -> {Column, Row},
 TableHeadings -> {None, {"Time\n (s)\n",
    "Position\n  (cm)\n", "TWall\n (K)", "Tpart\n (K)"}},
 TableAlignments -> Center];
```

Plot of Particle Temperature History

```
particleHistory = Join[allzone1, allzone2,
  allzone3, allzone4, allzone5, allzone6, allzone7];
historyplot = Transpose[Join[{Part[Transpose[particleHistory], 2]},
   {Part[Transpose[particleHistory], 4]}]];
ListPlot[historyplot, PlotJoined -> True,
 Frame -> True, FrameLabel -> {"Length (cm)", "Temp (K)",
   StringJoin["Particle Temperature at ", ToString[pOper],
    "Atm\nParticle Diameter= ", ToString[dp], " μm "], None},
 Ticks -> Automatic, ImageSize -> pagewidth]
Show[%, PlotRange -> {{30, 65}, {1760, 1880}}]
```